Quantifying the SST biases in data assimilative ocean simulations of the Benguela Upwelling System

Hermann Luyt
LYTHER001

Supervisors: Dr B.C. Backeberg (CSIR), Dr J. Veitch (SAEON) & A/Prof M. Vichi (UCT)

A minor dissertation submitted in partial fulfilment
of the requirements for the degree of
Master of Science
of the
University of Cape Town.

Department of Oceanography

February 2018

Declaration

I know that plagiarism is wrong. Plagiarism is to use another's work and pretend that it is one's own. I have used a Harvard-like convention for citation and referencing. Each contribution to, and quotation in, this minor thesis from the work(s) of other people has been attributed, and has been cited and referenced. This minor thesis is my own work. I have not allowed, and will not allow, anyone to copy my work with the intention of passing it off as his or her own work.

Signed: Signed by candidate

Date: 19 February 2018

Abstract

The Benguela Upwelling System (BUS) on the west coast of southern Africa is one of the global ocean's most productive upwelling systems supporting a large fishing industry, a fledgling aquaculture sector and offshore mining interests. Despite intensive monitoring and modelling studies, there is no regionally tailored ocean forecasting system that is explicitly developed to deal with the unique ocean dynamics of the Benguela. In this study, the Hybrid Coordinate Ocean Model (HYCOM) is used in conjunction with the Ensemble Optimal Interpolation (EnOI) assimilation scheme to study the impact of assimilating sea surface temperature (SST) and along-track sea level anomalies (SLA) observations on predicted upwelling dynamics in the Benguela. In order to evaluate the predictive skill and impact of data assimilation, three experiments with HYCOM-EnOI are evaluated: (1) with no assimilation ($\text{HYCOM}_{\text{FREE}}$), (2) only assimilating along-track SLA ($\text{HYCOM}_{\text{SLA}}$) and (3) assimilating both SLA and SST ($\text{HYCOM}_{\text{SLA+SST}}$). Using MODIS Terra SST as reference, the model SST outputs are evaluated. $\text{HYCOM}_{\text{FREE}}$ is found to exhibit a warm bias along the coast, $\text{HYCOM}_{\text{SLA}}$ shows an even greater warm bias while $\text{HYCOM}_{\text{SLA+SST}}$ conversely shows a much improved SST forecast skill. It is hypothesised that the warm biases could be due to errors in boundary conditions and/or the ERA-interim wind product used to force the model. Furthermore, a comparison of the assimilated SST product (the Operational Sea Surface Temperature and Sea Ice Analysis; OSTIA) with MODIS SST reveals biases in OSTIA up to $\pm 1°\text{C}$, raising questions over its suitability for assimilation in upwelling regions. Studying the effect of assimilation on SSH, SST and surface currents before and after the assimilation suggests that an increase in SSH from assimilated SLA leads to increased warm SST biases in $\text{HYCOM}_{\text{SLA}}$. This is due to an incorrect relationship between SSH and SST in the free-running HYCOM, from which the static ensemble is derived for the EnOI. $\text{HYCOM}_{\text{SLA+SST}}$ exhibits slightly enhanced SSH increments but the associated increase in SST is significantly reduced by the assimilated SST, resulting in a reduction of the bias with very little impact on the current dynamics. This is reflected in the surface velocitiy increments, which are similar to or worse than that of $\text{HYCOM}_{\text{SLA}}$. Investigating the potential of HYCOM-EnOI as an operational forecasting system has revealed that the assimilation of SST and along-track SLA vastly improves modelled SST for the BUS upwelling. Errors in the free-running model, which constitutes the static ensemble, need addressing and comparisons between MODIS and OSTIA SSTs suggests that OSTIA may not be ideally suited for assimilation in the case of coastal upwelling, due to limitations in capturing the dynamics correctly.

Acknowledgements

I must thank Dr Björn Backeberg for always having an open door and entertaining my ramblings, questions and pleas for help. Giving me a place to sit and work on this thesis with other like-minded researchers and students, allowing me to discuss ideas and get alternative perspectives, has been hugely beneficial. Most of all, thanks must be given for helping me with this project in the form of explanations, guidance, code, corrections and inspiration.

I would also like to thank Dr Jennifer Veitch for really helpful guidance on the Benguela region, for instilling confidence in my writing and being willing to meet with Dr Backeberg and I at rather short notice.

And thanks must be given to my third supervisor, A/Prof Marcello Vichi, for agreeing to supervise me while already burdened with other students and administrative tasks at UCT.

I thank Dr Josefine Wilms for invaluable help in coding and both Marcel van den Berg and Dr Marjolaine Krug for help in obtaining data. Members of CSIR's TIPHOON project were also instrumental in guiding my thesis.

This project was funded by the National Research Foundation (NRF), without which this work and the attached degree would not have been possible.

Thank you to my cohabitants in our small office, *Das Uboot*, for coffee runs, coding help and especially relief in the form of tasty memes.

A big thank you must go to my family and the Henry family for encouragement, nourishment and prayers throughout the writing of this thesis. Your presence at my side has been crucial. Tahlia Henry, thank you for keeping me in one piece and showering me with care.

Finally, thank you to the Father of our Lord, Jesus Christ, apart from whom I can do nothing.

Contents

List of Tables

List of Figures

Chapter 1

Introduction

The south-west African coast adjacent to the Benguela Current, one of the world's four major eastern boundary currents, is a region known for coastal upwelling (Shannon 1985). Here, upwelling occurs along the western coast of South Africa and the coasts of both Namibia and southern Angola. Alongshore winds, through Ekman transport, drive warmer surface waters offshore and upwell colder, nutrient-rich waters from depth to the surface (Open University 1989). This fact, together with other features of this region, make the BUS an important economic zone.

The upwelled, nutrient-rich waters are an abundant food source for phytoplankton which, in turn, attract fish, thereby sustaining a lucrative fishing industry for both South Africa and Namibia (Hutchings 1992; Bianchi et al. 2001; FIH 2009). In fact, continental shelves, such as the shelf beneath the Benguela, are where most of the world's commercial fisheries are located due to proximity to estuaries and river mouths, the penetration of sunlight in relation to depth and due to the aforementioned upwelling (Talley et al. 2011). More specifically, regions of upwelling account for 25% of the gross global ocean fish catches even though these areas only cover 5% of the world oceans (Jennings et al. 2009). The Benguela also hosts spawning regions for the three primary species contributing to the South African industry catch (sardine, anchovy and horse mackerel) as well as rock lobster, which all support predators in the region including seals, Cape Gannets and penguins (Hutchings et al. 2009). Coupled with the high productivity in the region is a regular occurrence of harmful algal blooms and anoxic conditions which lead to fish mortalities and lobster walkouts, especially in the St Helena Bay area (Pitcher and Calder 2000). A flourishing aquaculture sector is also expanding within the region (Britz and Venter 2016). Furthermore, marine mining operations occur offshore on a daily basis in the search for diamonds on the continental shelf (Sakko 1998; Griffiths et al. 2005) and exploitation of the Kudu gas field 170 km west of Oranjemund (Boyer et al. 2000) and the Ibhubesi gas field offshore from Namaqualand is also expected in the near future (Berge et al. 2002; Nkomo 2009). Therefore, marine industries along the western coast of South Africa and Namibia stand to gain much from accurate forecasting and modelling of coastal upwelling and sea state in the Benguela region.

However, South Africa currently has no regionally tailored operational ocean model capable of accurately forecasting ocean conditions. Such a system would hold immense economic, physical, biological and meteorological importance (Shannon 1985; Hutchings

et al. 2009). Benefits include the ability to model ocean processes at the scale of a single bay or short stretch of coastline, storm surge predictions, forecasting oil spill trajectories, supporting sea rescue efforts, improving ship routing, enhancing fishing catch and predicting harmful algal blooms. These benefits meet the goals of Operation Phakisa-Ocean, a South African government initiative to grow the blue economy while safeguarding the marine environment (Department: Planning, Monitoring and Evaluation 2014).

A regional ocean circulation model that assimilates both satellite-derived sea surface temperatures (SST) and along-track sea level anomalies (SLA) is currently in development for South Africa's regional ocean (Backeberg et al. 2014). However, validation studies for this model have been focussed on the Agulhas Current region (Backeberg et al. 2014). Preliminary studies of the model in a forecast mode suggest a warm bias is present along the coastline adjacent to the Benguela (Luyt 2016). Possible reasons for this warm bias include wind stress anomalies (Koseki et al. 2018), the misrepresentation of wind stress from the use of a relatively low resolution wind product (Veitch et al. 2009), the overestimation of warm Agulhas Current water entering the region (Veitch et al. 2010) and biases in satellite SST used to validate model outputs (Dufois et al. 2012). There is, therefore, a need to accurately diagnose the model biases in order to improve its accuracy, reliability and usefulness as an operational ocean model for the Benguela Upwelling System, and the South African Exclusive Economic Zone in general.

The aim of this research is to understand and evaluate the ability of a regional Hybrid Coordinate Ocean Model (HYCOM, Bleck 2002) combined with the Ensemble Optimal Interpolation (EnOI, Oke et al. 2002) data assimilation scheme, to forecast upwelling dynamics in the Benguela. HYCOM in free-running mode (without data assimilation) shows a warm bias. In this study, the effect of incorporating SST and SLA assimilation in HYCOM using the EnOI will be investigated. To study the impact of data assimilation, output from three model experiments will be compared to reference satellite data. This comparison will reveal both the forecast skill of the model and biases in the outputs. The three experiments are (1.) no data assimilation, (2.) assimilation of along-track sea level anomalies (SLA) only, and (3.) assimilation of along-track SLA and sea surface temperature (SST) observations from the Operational Sea Surface Temperature and Sea Ice Analysis (OSTIA) product.

This thesis is structured as follows: Chapter 2 provides a summary of the Benguela Upwelling System (BUS) focussing on the geography and bathymetry, the wind and upwelling regimes and the circulation and transport features. A brief history of modelling and model assimilation in the region as well as in other upwelling systems around the world is also presented here. Chapter 3 describes the HYCOM model used, the EnOI assimilation scheme, the different datasets and the methods used to produce the results shown and discussed in Chapter 4. Concluding remarks are then presented in Chapter 5.

Chapter 2

Background

2.1 The Benguela Upwelling System (BUS)

The term 'Benguela Upwelling System' (BUS) is used in this study to refer to the cohesive whole of two parts: the eastern limb of the South Atlantic Sub-tropical Gyre referred to as the Benguela Current and the coastal region of cool, upwelled water referred to as the Benguela upwelling regime. The geographical extent of the BUS being focussed on in this study spans 6–21°E and 9–39°S.

2.1.1 Geographic and bathymetric contexts

Eastern boundary currents are weaker, slower, shallower and wider in comparison to their western boundary counterparts (Talley et al. 2011). The four major upwelling systems of the world, the most productive regions of the global ocean, all correspond with eastern boundary current systems: the Benguela Current, the Canary Current, The California Current and the Humboldt Current (Hill et al. 1998). Each of these currents constitute the eastern horizontal extremities of the great ocean gyres.

The Benguela Current system is unique in that it is bound by warm water current systems in both the north and the south (Shannon and Nelson 1996; Shannon and O'Toole 2003). The Angola Current in the north brings warm, equatorial water south along the western African coast and meets the Benguela at the Angola-Benguela Frontal Zone (ABFZ), occurring at ∼15–17°S (Shannon et al. 1987). To the south of the Cape Peninsula, the Benguela is bound by the Agulhas Current which releases eddies and filaments of warm, high-salinity water into the Benguela and southern Atlantic in regular events termed the Agulhas Leakage (de Ruijter et al. 1999).

The large-scale bathymetry of the BUS consists of two large basins, the Cape Basin in the south and the Angola Basin in the north, separated by the Walvis Ridge which runs from close to the coast (∼20°S) in a south-westward direction towards the Mid-Atlantic Ridge for over 2500 km (Shannon 1985). This ridge is a barrier to water flow in the northward and southward directions at depths exceeding 3000 m and impacts the circulation in the south-east Atlantic (Nelson and Hutchings 1983; Shannon 1985).

The bathymetry of the continental shelf varies along the coast, being widest near the Orange River mouth (180 km) and at the Agulhas Bank on the south of the continent while being relatively narrow at the Cape Peninsula (40 km), south of Lüderitz (75 km) and off Angola (20 km; Shannon 1985).

2.1.2 Wind regime

The prevailing winds in the BUS are equatorward, alongshore winds regulated by the South Atlantic High Pressure System (SAH), the prevailing adjacent continental pressure system and eastward propagating cyclone systems (Nelson and Hutchings 1983; Shannon 1985). The upwelling-favourable winds drive an Ekman transport that forces warmer surface waters offshore and upwells colder subsurface waters to the surface. These alongshore equatorward winds are guided by a thermal barrier created by the Namib Desert on the coast and by the mountain configurations of the continental escarpment (Shannon 1985). The SAH maintains a year-long presence with a seasonal oscillation between a more south-eastward position (∼30°S, 5°E) in the austral summer and a more north-westward position (∼26°S, 10°E) in the austral winter (Preston-Whyte and Tyson 1988). This seasonal shift causes a prevailing westerly wind in the southern Benguela (32–34°S) during winter but the equatorward southerlies remain dominant in the central Benguela (24–32°S) throughout the year blowing strongest during the summer season (Strub et al. 1998).

Passing cyclones forming before Rossby waves in the subtropical jet stream within the westerly wind belt (35–45°S) modulate upwelling-favourable winds in the southern Benguela (Shannon 1985; Shannon and Nelson 1996). The modulations, relaxing or reversing the upwelling-favourable winds, occur on timescales of about a week in the austral summer to a month in the austral winter (Jury et al. 1990). The vigour of the modulations is sensitive to the properties of the atmospheric Rossby waves propagating through the subtropical jet stream (Nelson and Hutchings 1983).

The upwelling-favourable conditions of the entire Benguela are also subject to a phenomenon termed ‘berg winds’. These are katabatic wind events which occur during austral autumn and winter and are associated with the development of large high pressure systems over the southern parts of the subcontinent (Shannon 1985). Berg winds persist for a duration of around four days and blow offshore, inhibiting upwelling (Nelson and Hutchings 1983).

2.1.3 Upwelling regime

Upwelling along the coast adjacent to the Benguela extends from ∼15°S, effectively the northern border of the upwelling regime, to Cape Agulhas at ∼35°S. Lutjeharms and Meeuwis (1987), through the use of satellite-derived SST for the period 1982–1985, identified eight localised upwelling cells in the BUS and named them the Cunene (17.5°S), Namibia (21°S), Walvis Bay (24°S), Lüderitz (27°S), Namaqua (30°S), Cape Columbine (33°S), Cape Peninsula (34°S) and Cape Agulhas (35°S) cells. Demarcq et al. (2003), also using satellite-derived SST but for the duration 1982–1999, created a SST climatology confirming the notion of regions of localised upwelling and documented the annual, monthly and seasonal upwelling variability of three distinct regions: Walvis Bay (22.5°S) to 28°S; the Hondeklip Bay area (∼30°S); North of Cape Columbine (∼33°S) to Cape Peninsula (34°S). In their annual climatology, a constant cool SST belt exists along the coast due to the presence of constant coastal upwelling activity. Average SST for the three upwelling regions were found to be <16.7°C from Walvis Bay to Cape Town and 17–18°C for the

intermediate upwelling regions above and below the Walvis-Peninsula coastal stretch (Demarcq et al. 2003). Beyond the constant cool waters at the coast a predominantly warm SST was observed offshore in the austral summer and in winter the cooler waters were observed further offshore. Demarcq et al. (2003) further observed minimal variability in upwelling along the Walvis-Peninsula stretch during the months of May to November (standard deviations <1°C) and increased variability during December to April (up to >2°C in February and March). However, they stress that this could be due to both seasonal changes in the southern Benguela and anomalous temperature events which occurred in the summer of 1999–2000 (see Roy et al. 2001), both of which would have been captured in their climatology.

The offshore extent of the band of cool coastal water, demarcating the upwelling front, generally follows the shelf edge along the coast (Shannon 1985). Its position along the shelf edge is relatively stable in the southern Benguela, however, the northern Benguela displays a more variable spatial distribution thereof (Shannon and Nelson 1996). Perturbations in the upwelling front occur in the form of well-documented features called filaments (Lutjeharms and Meeuwis 1987; Lutjeharms et al. 1991; Shillington et al. 1992). These features are generally shallow (∼50–100 m deep), extending 100–500 km offshore but have also been observed at extents of ∼1000 km offshore (Lutjeharms et al. 1991). Filaments typically occur near the Lüderitz and Namaqua cells (∼26–29°S) with predominantly perpendicular orientations to the coast (Lutjeharms and Meeuwis 1987; Shannon and Nelson 1996) and persist from several days to a few weeks (Lutjeharms et al. 1991). Longer filaments tend to meander (∼250 km in wavelength, ∼100 km in amplitude), a characteristic which is affiliated with the interaction with passing northward-moving Agulhas Rings which can also elongate the filaments even further offshore (Lutjeharms et al. 1991; Shillington et al. 1992). Ikeda and Emery (1984) theorise that complex wind forcings are an important driving factor in the formation of filaments, Lutjeharms et al. (1991) relates filament formation to the presence of strong, seaward berg winds and Shillington et al. (1992) attribute both enhanced wind stress and topography.

The upwelling front is also a region of cyclonic eddy generation. Eddies have been observed to form and advect offshore (Lutjeharms and Meeuwis 1987; Strub et al. 1998). In particular, the Cape Peninsula is prolific in the production of these eddies, also observed by Strub et al. (1998), and it has been proposed that their generation is initiated by filaments originating in the Agulhas Retroflection south of Cape Agulhas (Lutjeharms and Meeuwis 1987).

The Lüderitz upwelling cell, found at the geographical centre of the upwelling region, was found to exhibit the coldest average SST, greatest seaward extent (280 km average), highest upwelling occurrence and highest wind stress. The cell exhibits strong upwelling year-round (Lutjeharms and Meeuwis 1987) and due to its location and vigour is considered to be the centre of the upwelling regime (Stander 1964; Bang 1971; Parrish et al. 1983), splitting it into northern and southern components as an environmental barrier between them (Shannon 1985). The Lüderitz cell is most developed in autumn and its alongshore extent is at a maximum during austral winter and spring, extending into the Walvis Bay

area (Lutjeharms and Meeuwis 1987). This matured development is reflected in the lowest mean winter temperatures of 13°C compared to that of summer, 15°C, when the upwelling intensity for the cell is at its minimum (Parrish et al. 1983). Indeed, SSTs at the Lüderitz cell remain low, not reaching 18°C, not even during the warmer austral summer (Lutjeharms and Meeuwis 1987). In the annual climatology created by Demarcq et al. (2003), an intense temperature gradient was observed further west from the Lüderitz cell at 16°E. Approaching the coast from the west, temperatures dropped from 19.8°C to 13.2°C across this gradient, a difference of 6.6°C.

The upwelling cells to the north of the Lüderitz cell (Walvis Bay, Namibia and Cunene) show increasing mean temperatures with increasing distance northwards and also show a reduced seaward extent of upwelling (Lutjeharms and Meeuwis 1987). These cells display year-round upwelling, except for the northernmost Cunene cell which displays a seasonal signal analogous to the cells south of Lüderitz. The northern boundary of the Benguela occurs at the ABFZ just north (∼15–17°S) of the Cunene cell (17.5°S). Fluctuations in upwelling-favourable wind stress are responsible for the seasonal intensity of the ABFZ and its location is related to the impact of wind stress curl on the poleward flow associated with its northern boundary (Colberg and Reason 2006). Rapid, short duration warm water intrusions into the northern Benguela occur across this barrier (Mohrholz et al. 2004; John et al. 2004) and warmer Angolan waters enter into the system through a poleward undercurrent (Mohrholz et al. 2008) mixing with and warming subsurface waters before upwelling.

Moving south from the Lüderitz cell, an increasing mean temperature in the cells with latitude is displayed, mirroring the trend in cells when moving north from the Lüderitz cell (Lutjeharms and Meeuwis 1987). Seaward extents also diminish, but the Columbine cell demonstrates a maximum extent compared to the other southern cells. As mentioned in §2.1.2, the seasonal shift of the SAH relaxes the upwelling-favourable winds in the southern Benguela during the austral winter and westerly winds dominate, creating a strong seasonal signal. This leads to a maximum in upwelling for the Cape Columbine, Cape Peninsula and Cape Agulhas cells in the spring and summer months (Shannon 1985; Lutjeharms and Meeuwis 1987).

2.1.4 Circulation features

The 200–300 km wide Benguela Current, forming the eastern limb of the South Atlantic Sub-tropical Gyre, flows northwards in its southern extent and then tends to a north-westerly direction moving northwards until parting from the coast at ∼24–30°S (Shannon 1985; Reid 1989). Where the Benguela leaves the coast, there is a divergence of the flow and one to two smaller branches of the current continue along the coast towards the ABFZ (Moroshkin et al. 1970). Between 23°S and 15°S, the surface waters exhibit a considerable westward flow and north of this region there exists the cyclonic Angola Gyre, 2000 km in diameter, with the Angola Current comprising its eastern extent (Moroshkin et al. 1970; Gordon and Bosley 1991). Where the poleward flowing Angola Current and the equatorward flowing Benguela converge culminates in the westward flow (Gordon and Bosley 1991). The features mentioned here are shown in Figure 2.1.

A further notable surface circulation feature is the Goodhope Jet. This equatorward jet current was first theorised due to intense horizontal density gradients before being observed and described by Bang and Andrews (1974). This jet current is perennial, with a speed of $\sim$50 cm.s^{-1} and a width of 20–30 km. Its constant presence is, however, affected by very seasonal wind forcing and barotropic shelf waves (Boyd and Nelson 1998) contributing to seasonal intensification. However, this seasonal effect is somewhat masked by Agulhas water influx.

Finally, as mentioned in §2.1.3, there exists a poleward undercurrent. The undercurrent flows along the coast west of the shelf break (Moroshkin et al. 1970; Nelson and Hutchings 1983) and has been shown to penetrate as far south as the Cape of Good Hope (Nelson 1989).

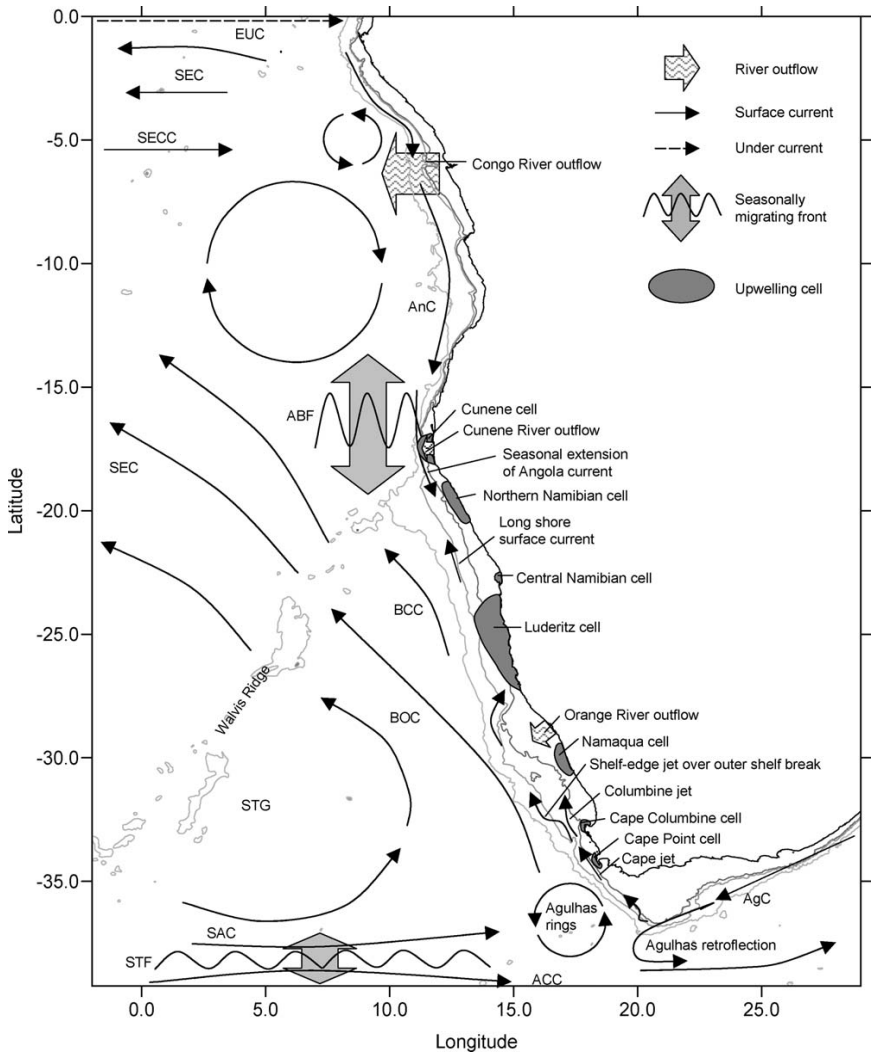

Figure 2.1: Physical features of the BUS, where: EUC is the Equatorial Under Current; SEC is the South Equatorial Current; SECC is the South Equatorial Counter Current; AnC is the Angola Current; BOC is the Benguela Oceanic Current; BCC is the Benguela Coastal Current; SAC is the South Atlantic Current; AgC is the Agulhas Current; ABF is the Angola-Benguela Front; STF is the Subtropical Front; STG is the Subtropical Gyre; and ACC is the Antarctic Circumpolar Current. Source: (Hardman-Mountford et al. 2003)

2.2 Modelling and data assimilation in upwelling regions

2.2.1 Modelling and assimilation in other upwelling regions

The Benguela Current System forms one of four eastern boundary upwelling systems (EBUSs), the four largest upwelling systems in the world (Talley et al. 2011). The other three are associated with the California Current in north-western America, the Humboldt Current in south-western America and the Canary Current in north-western Africa. What follows is a summary of a few of the modelling studies conducted in these EBUSs.

Past modelling studies in the California EBUS include harnessing of a nested Innovative Coastal-Ocean Observing Network (ICON) program model with data assimilation in the Monterey Bay area by Shulman et al. (2002). This bay-scale, curvilinear grid model had a horizontal resolution of 1–4 km, 30 vertical layers and was coupled to and nested within a Pacific West Coast ICON model. Shulman et al. (2002) found that nesting of the finer scale ICON model in the PWC model vastly improved correlation between modelled and ADCP observed currents and improved the skill of forecasting the location and intensity of upwelling events. Assimilation of SST was beneficial for skin temperatures in the regional PWC model, but for assimilation in the finer scale ICON model variable heat fluxes as surface boundary conditions are necessary for accurate vertical thermal structure prediction. Shulman et al. (2009) assimilated Spray and Slocum gliders into a nested Navy Coastal Ocean Model (NCOM, Martin 2000) of Monterey Bay with a curvilinear grid at a horizontal resolution of 1–4 km. Assimilation of the glider data improved forecasts 1–1.5 days into the future with more accurate atmospheric forcing being deemed necessary for extended forecasts. The assimilation improved modelled SST and salinity during upwelling and relaxation periods both on the surface and in the vertical structure compared to an unassimilated model run with both models evaluated against mooring and remotely sensed data (Shulman et al. 2009). In the central California system, Penven et al. (2006) used a 1-way nesting approach with the Regional Oceanic Modelling System (ROMS, Shchepetkin and McWilliams 2005) model. A finer-resolution model was nested within a coarser-resolution model with the goal of capturing both near-shore finer scale dynamics and offshore coarser scale dynamics, respectively. This method resulted in minimal boundary discontinuities and valid representation of the local upwelling structure at a computational cost only marginally above that of the nested model alone (Penven et al. 2006). Also modelling the Monterey Bay area, Chao et al. (2009) used a triple nested ROMS setup with the finest resolution model being at a resolution of 1.5 km. Satellite SST and SSH along with *in situ* data were assimilated into the model using the 3DVAR algorithm resulting in a RMS difference of 1.5°C and 0.2 PSU when reanalyses and observations were compared for temperature and salinity respectively (Chao et al. 2009). Broquet et al. (2009), also utilising ROMS, assimilated satellite observations of the sea surface and *in situ* observations using the Incremental Strong constraint 4D-Variational (IS4DVAR) data assimilation system. This model spanned the entire California Current system and was run at both 1/10° and 1/3° in separate experiments with and without assimilation taking place. Broquet et al. (2009) found that assimilation reduced the difference between the model and observations by more than a factor of 2 and assimilations resulted in improved

modelling of the circulation up to 14 days after the assimilation cycle, showing promising results for an operational forecast and analysis system based on the model and assimilation method (ROMS-IS4DVAR). In an attempt to improve estimates of Ekman transport and pumping, mean current structure, water masses, stratification and associated variability along the western coast of the US and the California Current, Broquet et al. (2011) applied corrections to surface forcing and initial state during each assimilation cycle using ROMS-IS4DVAR. This resulted in improved ocean state and surface forcing. However, when only changing initial conditions like other assimilation schemes do, 4DVAR sometimes introduces questionable features. Allowing increments to the surface forcing reduced circulation errors, but at the expense of surface forcing degradation (Broquet et al. 2011). Zamudio et al. (2008), using a regional Hybrid Coordinate Ocean Model (HYCOM, Bleck 2002) of the southern Gulf of California nested within a Pacific and global HYCOM, isolated the effects of local winds and oceanic remote forcing to study their impact on eddy generation in the region. The regional model included 32 vertical layers and did not assimilate ocean observations. Zamudio et al. (2008) found that local wind is not as essential for eddy generation as the oceanic remote forcing. Zamudio et al. (2011) nested a 32 layer regional HYCOM of the northern Gulf of California in a global HYCOM to study seasonal and interannual variability of salinity in the region. It was found that evaporation alone could not explain the low-salinity water in the region for 2006 and 2008, but that coastally trapped waves intensifying the poleward current were responsible for the transport of large amounts of low-salinity waters into the region (Zamudio et al. 2011). HYCOM has also been used for studying the effects of the 1997–1998 El Niño (López et al. 2005) and 2001 Hurricane Juliette (Zamudio et al. 2010) on the Gulf of California.

In the Humboldt Current, sometimes called the Peru-Chile Current, Escribano et al. (2004) diagnosed coastal currents in the vicinity of Peninsula Mejillones, a major upwelling region, with a 3D model using the finite element method. Coastal eddies and reversal currents were found to be present while alongshore currents dominated the coastal circulation. Escribano et al. (2004) concluded that physical barriers could form due to interactions between water masses, upwelling plumes and alongshore currents, leading to semi-enclosed habitats. Penven et al. (2005) devised a ROMS model to examine the mean circulation, mesoscale dynamics and seasonal cycle of the Peru Current System, the northern constituent of the Humboldt Current. The ROMS had a horizontal resolution of $1/9°$, 32 vertical layers and boundary forcings were derived from climatologies. The model reproduced the major equatorward, counter- and under-currents in the region as well as the upwelling front, the equatorward cold water tongue and the equatorial front (Penven et al. 2005). Combes et al. (2009) used a coarser (20 km) resolution ROMS to investigate the variability of the entire Humboldt Current in combination with a tracer experiment to examine regional upwelling dynamics. Their study found that off the coast of Peru and at central Chile, the El Niño Southern Oscillation (ENSO) strongly modulates coastal upwelling due to the propagation of downwelling equatorial Kelvin waves rather than local wind stress (Combes et al. 2009). Shinoda and Lin (2009) investigated interannual variability in the upper ocean in regions on the coast of Peru and northern Chile where there is persistent

cloud cover. A HYCOM model with 16 vertical layers and forced with satellite-derived surface heat fluxes and surface winds was used to model the upper ocean dynamics. Shinoda and Lin (2009) found HYCOM to reproduce the SST and SSH variations of the region well and found that ENSO events play an important role in SST variability and heat flux. Furthermore, upper ocean dynamics were found to have a strong influence in controlling interannual SST variability north of 20°S. Using ROMS, Echevin et al. (2011) tested the model sensitivity to boundary conditions in the northern Humboldt Current. The model received boundary conditions from three ocean general circulation models (OGCMs) in three separate experiments. Current variability was found to be strongly dependent on timing and amplitude of equatorial waves while upwelling and equatorward flow were found to be influenced by nonlinear processes such as mesoscale eddies (Echevin et al. 2011). The effects of intraseasonal equatorial Kelvin waves on mesoscale eddy activity off Chile and Peru was studied by Belmadani et al. (2012), also using ROMS. The model had 32 vertical layers and was considered to be eddy resolving. The model was shown to successfully reproduce local variability and propagation of equatorial waves along the waveguide. Coastal eddy kinetic energy was found to increase in relation to Kelvin wave activity present at the model boundary and this effect was suggested to be a robust feature (Belmadani et al. 2012). The Humboldt Current's sensitivity to global warming was investigated by Echevin et al. (2012), who used a ROMS model that was forced at the ocean-atmosphere by a climate model, comparing pre-industrial and quadrupled CO_2 levels. The intensification of CO_2 lead to a powerful increase of the surface density stratification, a narrower coastal jet, an intensified undercurrent and an intensification of coastal turbulence (Echevin et al. 2012).

In the Canary EBUS, Johnson and Stevens (2000) used a fine resolution Canigo regional model of the area between the Canary Islands, the Azores and the Gibraltar outflow. The model was used to better understand *in situ* and remotely sensed data of the region as part of the multi-disciplinary CANIGO project. The model was found to represent the area well and reproduced currents, variability, associated upwelling and cool water filaments (Johnson and Stevens 2000). Also using the Canigo model, Stevens and Johnson (2003) studied the formation of upwelling filaments off the north-west African coast. Filaments were found to form in four preferred locations along the coast and their generation was theorised to be through the same mechanism as those in the California EBUS. While not a study on the Canary EBUS itself, the region was used by Martinho and Batteen (2006) in an attempt to reduce the pressure gradient force error observed in sigma coordinate models by reducing the slope parameter. Batteen et al. (2007) used a terrain-following Princeton Ocean Model (POM, Mellor 1998) to reproduce features in the northern Canary Current. Using process-oriented experiments, it was shown that numerical and physical choices in models are of great importance (Batteen et al. 2007). Using a 32 layer ROMS model, Mason et al. (2011) studied seasonal variability of the Canary Current. The seasonal variability of the current was found to be imparted by two large counterrotating anomalous features that form once annually and propagate westwards. Through sensitivity experiments, variability in wind stress curl was determined to be an important generating mechanism of

these features, but annual reversals of the boundary flow also played a role (Mason et al. 2011). Revisiting the Canary upwelling filaments, Troupin et al. (2012) improved on previous studies by more accurately representating the filament off Cape Ghir using a ROMS model. Their suggested mechanism of filament formation was the balance of potential vorticity in the region which can be applied to other EBUSs.

2.2.2 Modelling and assimilation in the BUS

Modelling of the BUS started with van Foreest and Brundrit (1982) who developed a continuously stratified, linear two mode numerical model for the southern Benguela. The modelled region extended from 70 km south of the Cape Peninsula to north of St Helena Bay and over 150 km offshore. The model was forced with constant upwelling-favourable wind for 3 days and produced local features, including the Goodhope Jet, but the frontal zones were lacking due to the linear character of the model (van Foreest and Brundrit 1982). Lutjeharms et al. (1995) made a first attempt at modelling the entire south-east Atlantic upwelling region using the Fine Resolution Antarctic Model (FRAM) at a resolution of 1/2° in longitude by 1/4° in latitude. Main large-scale upwelling processes and features were modelled well, including the upwelling centres and plumes (Lutjeharms et al. 1995). Following the use of the Norwegian Ecological Model (NORWECOM, Skogen and Søiland 1998) in the North Sea, Skogen (1999) validated its implementation in the BUS by reproducing some of the main regional features. The model was able to reproduce the upwelling cells, the ABFZ, the thermal front, the equatorward Benguela current and the poleward undercurrent (Skogen 1999). Studying the fish larvae retention processes in the upwelling plume at St Helena Bay, an important nursery ground on the western coast of South Africa, Penven et al. (2000) used an idealised barotropic model to investigate the regional oceanic processes. The model was based on the barotropic element of the SCRUM model (Song and Haidvogel 1994), neglecting density variations but solving the vertically integrated momentum equations. At a spatial resolution of 5 km, the model was able to reproduce a cyclonic eddy in the lee of Cape Columbine, driven by alongshore winds, acting as a retention mechanism by creating a dynamic boundary between the inshore and offshore regions (Penven et al. 2000). Continuing in the investigation of larval transport by physical processes to the St Helena Bay nursery grounds, Penven et al. (2001) devised a 3D regional configuration of the ROMS model for the southern Benguela. The model spanned the domain 28–40°S and 10–24°E and the grid was pie-shaped. The horizontal resolution was higher at the coast and the model was run twice: with a spatial resolution at the coast of ∼18 km in the first run to test the stability and robustness of ROMS in a regional configuration and ∼9 km in the second run to resolve mesoscale circulation features. The model was able to reproduce the upwelling plumes, filaments, eddies and nearshore circulation features crucial to regional ecological processes (Penven et al. 2001). This ROMS configuration of Penven et al. (2001), forced by comprehensive ocean and atmosphere dataset (COADS) monthly mean climatologies, has been named the 'PLUME' configuration and has been used in physical-biological model coupling studies (Mullon et al. 2002; Parada et al. 2003; Koné et al. 2005). Also using the PLUME configuration, Blanke et al. (2002) investigated the impact of wind on upwelling variability in the southern Benguela. It was

found that the coast north of Cape Columbine is sensitive to fluctuations in the open-sea winds and correlations between the model and observations made a case for studying anomalous events using regional numerical tools (Blanke et al. 2002). Similarly, Blanke et al. (2005) used ROMS in PLUME configuration and forced with QuickSCAT winds to diagnose the main scales of wind forcing pertinent to anomalous SST events in the southern Benguela. The temporal resolution of the wind forcing was found to be a crucial factor in reproducing the interannual SST anomalies when evaluating the model against NASA Pathfinder observations. Upwelling indices were also calculated to study the coverage and intensity of warm and cold events along the coast (Blanke et al. 2005). Equilibrium dynamics of the BUS were investigated by Veitch et al. (2009) and Veitch et al. (2010) using a regional ROMS model of the entire Benguela system. The model spanned 12.1–35.6°S and 3.9–19.8°E with a spatial resolution that ranged from 7.5 km in the south to 9 km in the north and had 32 vertical layers. The model reproduced all the salient features of the BUS, but a cold bias existed at the shore due to underestimation of local wind drop-off and a warm bias existed offshore due to an overestimation of warm Agulhas Current waters entering the BUS (Veitch et al. 2009). Veitch et al. (2010) observed the dynamics of the poleward countercurrent and its offshore deviation as well as the Benguela equatorward current and its bifurcation into a topographically controlled coastal limb and an offshore limb with a meandering nature moderated by passing Agulhas eddies. Fennel et al. (2012), using a very idealised Modular Ocean Model (MOM, Griffies et al. 2009), demonstrated the role of wind stress variations in explaining the circulation features of the BUS. Even though the model was idealised, it was useful in explaining the response of the equatorward flow and poleward undercurrent to variations in the wind stress. Mohrholz et al. (2014), also using MOM, *in situ* and satellite observations investigated cross shelf hydrographic and hydrochemical conditions in the northern Benguela. The model results confirmed the dependence of upwelling strength on coastal and wind curl uwpelling mechanisms. Tim et al. (2015) used a Max-Planck-Institute Ocean Model (MPI-OM, Marsland et al. 2003) in a global simulation at 0.1° resolution with focus on the BUS. The model was driven by atmospheric fields with the aim of finding the large-scale atmospheric drivers of variability and trends in upwelling. Though there were minor differences between the northern and southern Benguela, the correlations indicated the common atmospheric patterns that favour upwelling, namely the alongshore equatorward wind stress, the subtropical high pressure and an ocean-land sea level pressure gradient (Tim et al. 2015). Using the same ROMS configuration as Veitch et al. (2009), Machu et al. (2015) forced the model with surface forcings from a coupled atmosphere-ocean global circulation model at native resolution ($2.5° \times 1.3°$) and a downscaled resolution ($0.5° \times 0.5°$). The downscaled forcing improved physical and biogeochemical processes. The coarser native resolution forcing resulted in misrepresentations, including a shifted SST seasonality, but this and other features were corrected and improved when downscaling wind forcing (Machu et al. 2015). Junker et al. (2015) investigated the effect of wind stress curl on meridional advection in the northern Benguela using a regional numerical model based on MOM. The model was relatively coarse in the horizontal dimension with finest resolutions of 8 km at the coast. It was

found that the wind stress curl in this region could support a meridional advection southwards, transporting tropical waters into the BUS (Junker et al. 2015). Also using MOM, Schmidt and Eggert (2016) investigated oxygen dynamics in the BUS. While the focus was on physical-biological interactions, the upwelling and poleward undercurrent features, important in oxygen transportation, were well modelled. Renault et al. (2017) performed coupled ocean-atmosphere experiments by coupling a ROMS model to a Weather Research and Forecast (WRF, Skamarock et al. 2008) model for the southern African region, including the Benguela, Agulhas retroflection, Agulhas Current proper, the Mozambique channel and Madagascar. This study investigated the surface current feedback to the atmosphere and the resulting impact on the Agulhas Current retroflection and leakage. The feedback was found to reduce mesoscale energy by 25% and allow a larger leakage, changing the water masses of the BUS. Veitch and Penven (2017) investigated the impact of the Agulhas Current on the Benguela by comparing a standard ROMS simulation of the region with a ROMS simulation where the Agulhas was diverted so as to remove its influence on the Benguela. This model showed the warm water influence of the Agulhas beyond the shelf and an associated density gradient front. This gradient front was shown to influence coastal jets in the Benguela and the passing turbulence of the Agulhas leakage imparted powerful mixing on the upwelling front of the southern Benguela. However, regions of localised turbulence existed along the coast, independent of Agulhas influence.

Although operational products do exist for the global ocean, this study is the first assimilation experiment focussed on the Benguela region. Only the preliminary study of Luyt (2016) has evaluated the assimilated model outputs for this region prior to this study.

Chapter 3

Methods

3.1 HYCOM model

The Hybrid Coordinate Ocean Model (HYCOM), a primitive equation model, is a derivative of the Miami Isopycnic-Coordinate Ocean Model (MICOM), developed at the University of Miami (Bleck et al. 1992), and utilises the combined advantages of isopycnic-coordinate and fixed-grid ocean circulation models within a single framework (Bleck 2002). HYCOM overcomes challenges faced by fixed-coordinate models by changing between vertical coordinates: isopycnic (ρ) vertical coordinates when dealing with stratified open oceans, σ-coordinates when modelling shallow coastal regions, and z-level coordinates when dealing with dynamic, upper-ocean mixed layer events. The model determines the most favourable hybrid distribution at each time-step but will always favour the use of isopycnic coordinates where possible. Coordinates can locally deviate to σ- and z-coordinates where isopycnals fold, outcrop or produce an unsuitable vertical resolution in model regions (Chassignet et al. 2007).

3.1.1 Model setup and parameters

This study uses the same model instance developed by Backeberg et al. (2014) to primarily capture Agulhas Current mesoscale variability and dynamics. The BUS falls within the domain of this model so additionally evaluating the model's forecast skill in this region will further the effort to implement an operational ocean forecast model in the southern African region.

A regional implementation of HYCOM, nested within a validated, basin-scale HYCOM of the Indian and Southern Oceans was used (George et al. 2010). The nested HYCOM spans the the region 0–60°E and 10–50°S. The regional HYCOM receives boundary conditions from the basin-scale model at six-hourly intervals. Temperature, salinity, layer interface and baroclinic velocities are among the slowly changing variables relaxed across a 20 grid cell (∼200 km) transition region at the inner-outer model interface. At the boundary, the relaxation timescale is 13 hours and reduces by a factor of 4 as distance increases inwards. Barotropic velocities and pressure, faster changing variables, are dealt with using the Browning and Kreiss (1982, 1986) method of bounded derivatives at the inner model boundaries.

The grids of both models in the nested configuration were generated with the conformal mapping tool (Bentsen et al. 1999). The horizontal resolution of the basin-scale model

spans from 45 km in the Southern Ocean down to 14 km in the Indian Ocean, while the nested model has a resolution of $1/10°$(∼10 km). The region's Rossby radius of deformation is about 20–80 km (Chelton et al. 1998) and the inner model is considered to be eddy resolving. The models both have 30 hybrid vertical layers with a minimum thickness of 3 m in the uppermost layers.

The basin-scale model is initialised from Levitus climatology (WOA05; Locarnini et al. 2006; Antonov et al. 2006) and spun up for 10 years using ERA-interim forcing (Dee et al. 2011). The inner model is then initialised from a balanced field of the outer model interpolated to the higher resolution grid (∼10 km). Applying atmospheric forcing fields from the ERA-interim reanalysis data, the models are run from 1980 to 2007. Heat fluxes are recalculated as set out by Drange and Simonsen (1996) and momentum fluxes are determined using the accurate yet computationally efficient bulk formulas described by Kara et al. (2000). The TOTAL Runoff Integrating Pathways (TRIP; Oki 1998) hydrological model, receiving river run-off input from ERA-interim for a 20 year span, is used to estimate the monthly discharge from rivers. Rivers are considered to be negative salinity fluxes with additional mass exchange (Schiller and Kourafalou 2010). This salinity flux is applied to a layer, 6 m thick, to avoid instabilities close to river deltas being too great. This flux is dispersed over an area, half an ellipsoid in shape and 60 km by 200 km in size, across which the flux weighting reduces exponentially proportional to distance from the discharge point.

HYCOM version 2.2 (Wallcraft et al. 2009) has been used in this study. Further model parameters are listed in Table 3.1. For any further information on the model setup, see Backeberg et al. (2014).

For this study, the inner HYCOM was executed in three different modes: (1.) 'free-running' without data assimilation, henceforth $\text{HYCOM}_{\text{FREE}}$, (2.) assimilating along-track sea level anomalies (SLA), henceforth $\text{HYCOM}_{\text{SLA}}$, and (3.) assimilating both along-track SLA and sea surface temperature (SST), henceforth $\text{HYCOM}_{\text{SLA+SST}}$. The assimilation of data took place once a week (every seven days) and the model operated in a 'forecast' mode. The model ran in all three modes for the period spanning 1 January 2008–29 December 2009.

3.1.2 Data assimilation scheme

No numerical models perfectly represent the phenomena they are designed to replicate. Computational limits, parameterisations of variables, mathematical simplifications of complex events, inaccuracies in initial conditions and inaccurate boundary condition data and forcing fields are but a few sources of error in models. Error, furthermore, propagates through the model domain causing 'model drift', moving the representation of reality away from observations of the true state of the modelled phenomena. This drift can be restrained by regularly assimilating observational data into the model, resulting in an improved model estimate. In the realm of forecasting ocean conditions, data assimilation can be defined as the fusion of observational data into a dynamical model to enhance its forecast ability (Bertino et al. 2003).

In this study, the Ensemble Optimal Interpolation (EnOI; Oke et al. 2002; Evensen

Table 3.1: Additional model attributes sourced from Backeberg et al. (2014).

Model attributes	Values
Model state variables	Sea surface height, u- and v-component velocities, temperature, salinity, layer thickness
Horizontal resolution	1/10°
Vertical grid	30 hybrid layers
Target densities (+1,000 kg/m^3; layer 1 - layer 30)	22.30, 22.60, 22.90, 23.20, 23.50, 23.80, 24.10, 24.40, 24.70, 25.00, 25.30, 25.60, 25.90, 26.20, 26.50, 26.80, 26.89, 26.99, 27.08, 27.18, 27.27, 27.37, 27.46, 27.56, 27.65, 27.75, 27.84, 27.94, 28.00, 28.05
Reference pressure flag	Sigma-0
Minimum, maximum layer thickness for transition to z-level	3 m, 450 m
Topography	1' GEBCO
Atmospheric forcing	6-hourly ERA-interim
Boundary conditions	Unassimilated HYCOM of the Indian and Southern Ocean (George et al. 2010)
Advection scheme	2nd order
Vertical mixing scheme	KPP
Deformation-dependent biharmonic viscosity factor	0.20
Diffusion velocity (m.s^{-1}) for Laplacian momentum dissipation	0.005
Diffusion velocity (m.s^{-1}) for biharmonic momentum dissipation	0.06
Diffusion velocity (m.s^{-1}) for biharmonic thickness diffusion	0.005
Diffusion velocity (m.s^{-1}) for Laplacian temperature/salinity diffusion	0.005
Baroclinic time step	600 seconds
Barotropic time step	20 seconds

2003) assimilation scheme has been used. It is computationally more efficient than the Ensemble Kalman Filter (EnKF; Evensen 1994, 2003), which relies on a Monte Carlo integration step for sampling the forecast error covariance. The EnOI used in conjunction with HYCOM has been shown to replicate Agulhas Current dynamics with reasonable accuracy (Backeberg et al. 2008, 2009; Backeberg and Reason 2010; Backeberg et al. 2014) and the EnOI has performed well in other dynamically similar regions including the East Australia Current (Oke et al. 2007), the Gulf of Mexico (Counillon and Bertino 2009; Srinivasan et al. 2011) and the South China Sea (Xie et al. 2011; Lyu et al. 2014). Furthermore, the EnOI has been successfully used in the Northern and Baltic seas to assimilate temperature and salinity profiles (Fu et al. 2011) and in the Pacific to assimilate Argo profiles (Xie and Zhu 2010) and altimetry (Wan et al. 2010).

Data assimilation schemes always face the challenge of introducing observations into model equations. If one considers the data assimilation problem to be deterministic, it is overdetermined (Counillon and Bertino 2009). When solving the analysis, we can assume

that the observation error ($\boldsymbol{\epsilon}$) and forecast error ($\boldsymbol{\Upsilon}$) can be formulated as:

$$\mathbf{d} = \mathbf{H}\boldsymbol{\psi}^{\mathrm{t}} + \boldsymbol{\Upsilon}, \text{ and} \tag{3.1}$$

$$\boldsymbol{\psi}^{\mathrm{f}} = \boldsymbol{\psi}^{\mathrm{t}} + \boldsymbol{\epsilon}, \tag{3.2}$$

where $\mathbf{d}$ portrays the observations, $\boldsymbol{\psi}^{\mathrm{f}}$ the model forecast, $\boldsymbol{\psi}^{\mathrm{t}}$ the true state and $\mathbf{H}$ the measurement operator that relates the measurements to the forecasted model state variables.

The problem now becomes underdetermined but with an infinite number of solutions. Gaussian distributions of the errors ($\boldsymbol{\Upsilon}$ and $\boldsymbol{\epsilon}$) are assumed as well as a linear relationship between all the variables, in accordance with the method of Bertino et al. (2003). This allows for the calculation of a model analysis state ($\boldsymbol{\psi}^{\mathrm{a}}$) estimation using least-squares and minimises the difference from the truth, $\boldsymbol{\psi}^{\mathrm{t}}$ (Counillon and Bertino 2009).

The computational efficiency of the EnOI assimilation scheme arises in its creating only a single forecast member, as opposed to Monte Carlo methods which produce many forecast members. For Monte Carlo methods, the variance of the many members is representative of the forecast error. However, the EnOI estimates forecast error ($\boldsymbol{\epsilon}$) from a 'static ensemble' ($\mathbf{A} \in \mathbb{R}^{n \times N}$, where n is the model state dimension and N the ensemble size) and assumes climatological variability is representative of assimilation cycle error (Oke et al. 2002; Evensen 2003):

$$\overline{\boldsymbol{\epsilon}\boldsymbol{\epsilon}^{\mathrm{T}}} \approx \mathbf{C} = \frac{\alpha}{N-1}\mathbf{A}'(\mathbf{A}')^{\mathrm{T}}, \tag{3.3}$$

where $\mathbf{A}'$ is the centred historical ensemble (calculated as $\mathbf{A} - \overline{\mathbf{A}}$), N is the ensemble size and $\mathbf{C}$ is the system background error covariances. α ($\in (0, 1]$) is a scaling factor used to mitigate large seasonal or interannual variances which may occur when sampling an ensemble of model states over long time periods. These large variances are unsuitable for representation of the assimilation cycle error (Counillon and Bertino 2009). In similar fashion, the observations error covariance matrix is sampled as:

$$\overline{\boldsymbol{\Upsilon}\boldsymbol{\Upsilon}^{\mathrm{T}}} \approx \mathbf{R} = \frac{\alpha}{N-1}\mathbf{T}'(\mathbf{T}')^{\mathrm{T}}, \tag{3.4}$$

where $\mathbf{R}$ is the observation error covariance.

The static ensemble, $\mathbf{A}$, was created from the free-running, nested HYCOM sampled every five days throughout the period 1998–2007 (Backeberg et al. 2014). The model's spin-up preceding the sampling was of an adequate duration that model drift, a potential source of erroneous and artificial correlations, was avoided.

It is expected that the assimilation of SLA causes simultaneous hydrographic changes due to the correlation between sea surface height (SSH) and the water masses of mesoscale features. When Backeberg et al. (2014) explored correlations between SSH and SST for the entire 10-year ensemble duration, no relationship was found. There is, however, a strong seasonal variability to SST which impacts on the three-way relationship between SST, SSH and the corresponding ocean dynamics. In particular, there is a strong seasonal enhancement of the correlation (R = 0.4) in the winter months of June, July and August.

To limit the effect of seasonal variability on the EnOI correlation matrix, the static ensemble is adjusted to account for this seasonality. The adjusted ensemble now consists of a sixty-day moving window of ensemble states ($\mathbf{A}_{t0}$) centred at the appropriate seasonal time of year ($t0$) with respect to the time of assimilation (Xie et al. 2011). The adjusted ensemble consists of 120 members, relatively large in sample size, and limits the noise in the spatial correlation (Backeberg et al. 2014).

However, despite the substantial size of the static ensemble, it does not cover model variability over the entire domain and associated sampling errors produce artificial long-range spatial correlations. Often, a large problem from sampling historical covariance over a long period of time is that you may include long-term trends in the variability such as global warming and interannual or decadal variability. To reduce the effect of these correlations, the impact of the assimilated observation is spatially restricted using a local framework methodology (Evensen 2003). Backeberg et al. (2014) concluded that a localisation radius of 400 km is appropriate for the modelled region. After applying a Gaspari and Cohn function (Gaspari and Cohn 1999) to avoid discontinuities in the modelled forecast state update, a resultant effective localisation radius of ∼100 km is reached. The model state of the forecast ($\boldsymbol{\psi}_f$) is then updated through the multivariate properties of the EnOI.

The assimilation cycle then follows the sequence of Xie et al. (2011). The purpose of the investigation, as stated previously, is to evaluate the model in a forecast mode where assimilation occurs at the beginning of the 7-day forecast cycle. SSH is diagnosed from the model state, SLA is calculated by then subtracting the model mean and the assimilated SLA observations are used to correct the modelled SLA anomaly. This ensures that averaging the innovations (the difference between the model forecast and the observations) over many assimilation cycles converges to 0, but it does not address potential biases in the model variability error (Backeberg et al. 2014).

A first guess approach (FGAT) is employed where the model forecast ($\boldsymbol{\psi}^{\mathrm{f}}$) and the observations ($\mathbf{d}$) are compared on the same day ($t0 - i$, where i represents the day in the 7-day forecast cycle). The assimilated analysis state ($\boldsymbol{\psi}^{\mathrm{a}}_{t0}$) is then estimated:

$$\boldsymbol{\psi}^{\mathrm{a}}_{t0} = \boldsymbol{\psi}^{\mathrm{f}}_{t0} \sum_{i=0..6} \mathbf{A}'_{t0}(\mathbf{A}'_{t0})^{\mathrm{T}}\mathbf{H}^{\mathrm{T}} \left(\mathbf{H}\mathbf{A}'_{t0}(\mathbf{A}'_{t0})^{\mathrm{T}}\mathbf{H}^{\mathrm{T}} + \left(\frac{N-1}{\alpha} \right) \mathbf{R} \right)^{-1} (\mathbf{d}_{t0-i} - \mathbf{H}\boldsymbol{\psi}^{\mathrm{f}}_{t0-i}), \tag{3.5}$$

where $\mathbf{H}$ is the measurement operator that relates the measurements to the forecasted model state variables and $\mathbf{R}$ is the observation error covariance matrix (see Equation 3.4). For computational efficiency and ease, the observation error covariance matrix ($\mathbf{R}$) is considered to be a diagonal matrix and its variance is determined as proposed by Oke et al. (2008):

$$\epsilon^2_{\mathrm{o}} = \epsilon^2_{\mathrm{instr}} + \epsilon^2_{\mathrm{re}}, \tag{3.6}$$

where ϵ^2_{o} is the observational error variance, $\epsilon^2_{\mathrm{instr}}$ is the instrument error and ϵ^2_{re} is the representativity error. The representativity error, similar to tuning α, was set to a value of 1 to keep the tuning process simple (Backeberg et al. 2014).

Table 3.2: Altimetry missions in operation for study time period.

Altimetry mission	Study coverage
GFO	January 2008–September 2008
Jason-1 (old orbit)	January 2008–October 2008
Jason-2	October 2008–December 2009
Jason-1 (new orbit)	February 2009–December 2009
Envisat	January 2008–December 2009

3.1.3 Assimilated data

$\text{HYCOM}_{\text{SLA}}$ and $\text{HYCOM}_{\text{SLA+SST}}$ both assimilated delayed-time, unfiltered along-track SLA from satellite altimeters. These data were produced by SSALTO/DUACS and previously distributed by Aviso+, now available from Copernicus Marine Environment Monitoring Service (CMEMS).

The gridded SLA level 4 product was not used because the interpolation scheme employed to generate the gridded product in the large, unsampled regions of the ocean and its associated smoothing could mean regions with rapidly changing dynamics are underrepresented or contain unrealistic features (Ducet et al. 2000; Traon and Dibarboure 2004). It has been shown, however, that an increase of concurrent altimeter missions results in more accurate level 4 SLA products (Pascual et al. 2006). The unfiltered, along-track data are adequate for sampling the finer spatial scales related to eddies (Wunsch and Stammer 1998) and exhibit reduced aliasing in the SLA signals (Byrne and McClean 2008).

The delayed-time product uses the Geophysical Data Record (GDR) computed from a precise orbit ephemeris to apply altimetric corrections to the altimeters. Each altimeter is further homogenised using a model and reference. Hereafter, a repeat-track analysis is performed followed by the subtraction of a mission-unique mean profile from the data to estimate the SLA (Dibarboure et al. 2011).

The SLA data have a horizontal resolution of 7 km. The altimeters in operation during the temporal range of this study are listed in Table 3.2.

$\text{HYCOM}_{\text{SLA+SST}}$ assimilated SST from the Operational SST and Sea Ice Analysis (OSTIA) product in addition to along-track SLA. This is a daily, global gridded SST analysis derived from an amalgamation of satellite and *in situ* observations at a $1/20°$($\sim$5 km) horizontal resolution (Donlon et al. 2012). The OSTIA analyses are produced by the United Kingdom Met Office (UKMO) and are available from CMEMS. Only the analysis corresponding to the day of assimilation is assimilated into the model. The analyses for the remaining weekdays are not assimilated.

In order to create a global level 4 product, OSTIA assimilates the many observations (see Table 3.3), differing in both time and space, using optimal interpolation (OI) (Martin et al. 2007). OSTIA uses a persistence approach where the previous analysis field is used as a background field from which a background error covariance matrix is generated and in the absence of new observations the background is relaxed towards a climatology (Donlon et al. 2012). Using the background field, the background error covariance matrix and any new observations, the analysis is produced using OI and solved with the Analysis Correction

Table 3.3: Observation sources used in OSTIA, sourced from Donlon et al. (2012).

Sensor	Sensor type	Resolution	Coverage
ENVISAT AATSR	Infrared	∼1.1 km (swath)	Global
AVHRR—LAC European North Atlantic Area (NAR)	Infrared	∼0.1° (gridded)	North-East Atlantic and Mediterranean
AVHRR—LAC	Infrared	∼1.1 km (swath)	Various regions depending on the data availability at the time
AVHRR—GAC	Infrared	∼8.8 km (swath)	Global
MetOP AVHRR	Infrared	∼1.1 km (swath)	Global
MSG SEVIRI	Infrared	0.1° (gridded)	Atlantic sector
Aqua AMSR-E	Microwave	∼25 km (swath)	Global
TRMM TMI	Microwave	∼25 km (swath)	Tropics
In situ temperature and salinity	Ships; drifting and moored buoys	*In situ* point sample	Global
Sea ice concentration	Passive microwave	10 km	Global (northern and southern hemisphere maps)

method (Lorenc et al. 1991; Martin et al. 2007).

3.2 Reference data

SSTs from the Moderate Resolution Imaging Spectroradiometer (MODIS) aboard the NASA Terra platform was selected as a reference dataset to compare the model outputs and OSTIA to. The global, mapped level 3 product is created by the NASA Ocean Biology Processing Group (OBPG) and is available from NASA's Physical Oceanography Distributed Active Archive Center (PODAAC).

The designated requirements for noise equivalent temperature difference (NEDT) of MODIS thermal infrared bands is 0.05°K, a considerable advancement over its predecessor, the Advanced Very High Resolution Radiometer (AVHRR) which exhibited an NEDT of 0.12°K (Goodrum et al. 2000). MODIS possesses an array of 36 observed spectral bands of which some are dedicated to the sensing of atmospheric properties such as cloudcover and aerosols. This allows for improved atmospheric correction and cloud masking, resulting in more reliable SST observations. The MODIS sensor is borne upon both NASA's Terra and Aqua satellite platforms. When compared to buoys and ship-borne infrared radiometers, MODIS Terra has been shown to be of an accuracy suitable for research and operational implementations (Minnett et al. 2002, 2004). As such, MODIS SST products have been used in the study of large lakes in the United States (Crosman and Horel 2009), Sweden (Reinart and Reinhold 2008) and in the Curonian Lagoon of the Baltic Sea (Kozlov et al. 2014). Hao et al. (2017) summarised *in situ* validation studies of MODIS SST showing the Terra platform's sensor, as opposed to the Aqua sensor, to be in better agreement with *in situ* observations both in the literature and in their own validation study in the coastal waters of the Yellow Sea. Qin et al. (2014), while validating MODIS SST in the South China Sea, also demonstrated the ability of the sensor to detect smaller oceanic features

such as oceanic fronts and coastal upwelling.

The MODIS Terra SST level 3 product used in this study contains daily observations spanning both the spatial and temporal domains of the area of interest. Terra is in a near-polar, sun-synchronous orbit at an altitude of 705 km with a 10:30 am local descending equatorial crossing. The SST field was captured using the 3 and 4 mid-infrared bands (channels 20, 21, 22 and 23) with wavelengths ranging 3.66–4.08 µm and has a spatial resolution of 4.63 km. This dataset is the nighttime product which is appropriate for model validation because of the absence of diurnal heating of the ocean skin temperature captured by nighttime observations from the sensor.

3.3 Comparing model to reference satellite data

3.3.1 Data preparation

Before comparisons to the reference MODIS dataset were made, all datasets were first homogenised. Spatial resolution, cloud cover and missing satellite data were considered in this homogenisation.

The HYCOM outputs, OSTIA and MODIS each have differing native spatial resolutions. In order to make meaningful conclusions from their differences, the datasets first needed to be interpolated to the coarsest resolution among the datasets. The HYCOM outputs exhibit the lowest resolution (∼10 km), so OSTIA and MODIS were regridded using a nearest neighbour interpolation to assign SST values to the new grid points.

MODIS level 3 SST data are masked in regions where observations are obscured by cloud. Cloud-free days in the study area are at a minimum in the lower latitudes, both offshore at the Angola-Benguela Frontal Zone (∼15–17°S) and along the Namibian coastline (Figure 3.1). The regions surrounding the South African coastline are least affected by cloud in this period.

A daily cloud mask was extracted from the regridded MODIS dataset and applied to all the HYCOM outputs and the OSTIA dataset. This ensured that effects from cloud cover in the reference dataset were not creating spurious results when compared with HYCOM and OSTIA.

Over the days of 21–23 December 2008, no data for MODIS Terra is available. The sensor had a fault over this time so the respective days were also removed from the other datasets.

An initial look at the differences between OSTIA and MODIS is shown in Figure 3.2. Warm biases in OSTIA of 0.25 to 0.75°C are seen offshore and in the northern (10–15°S) and southern (35–40°S) regions of the study area. A cool bias (-0.50 to -0.25°C) exists close to shore in the northern Benguela in the 2-year means. The winter differences show a similar bias in the north (10–25°S) while summer differences show a cold bias much further south (22–32°S). These preliminary results suggest that OSTIA may not be the optimal SST product for use in assimilation.

3.3.2 Mean state and variability

In order to evaluate the ability of HYCOM to resolve upwelling SST dynamics in the Benguela it needs to be evaluated against reference data. The model operating in ‘free-run’,

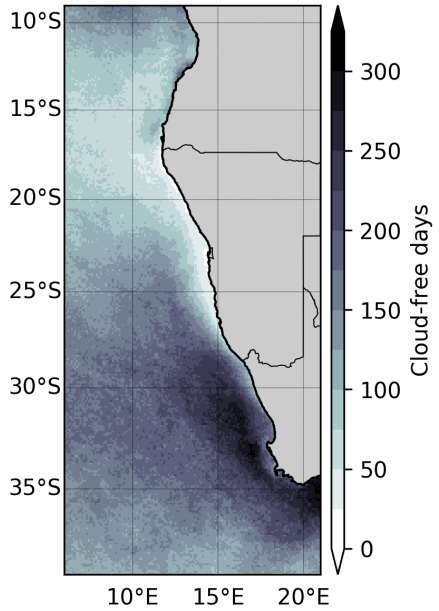

Figure 3.1: MODIS cloud-free days for the temporal range of the study.

$\text{HYCOM}_{\text{FREE}}$, and its two assimilated counterparts, $\text{HYCOM}_{\text{SLA}}$ and $\text{HYCOM}_{\text{SLA+SST}}$, are simultaneously compared to MODIS, the reference dataset.

Firstly, 2-year mean SST plots are created for each dataset. Differences between these means and the mean reference dataset are then calculated and mapped. These highlight the mean, 2-year, differences between the datasets. 2-year standard deviations are also calculated and mapped for each dataset. This reveals the ability of the model outputs to represent daily variability at the ∼10 km scale and how they fare between each other at this skill.

Seasonal means are then created for each product. A summer mean encompassing the months of January, February and March (JFM) and a winter mean encompassing the months of June, July and August (JJA). Summer and winter seasonal means are created for the period 2008–2009 before being compared to the seasonal reference datasets. The same procedure is followed for the standard deviations. These facilitate an evaluation of the ability of the model to represent seasonal features and variabilities.

3.3.3 Increment analysis

In order to better understand the net impact of assimilation on the model and its outputs, an 'increment analysis' is performed. Here, increment refers to the net change in variables that occurs as a result of assimilation. It is calculated by subtracting the model state after assimilation from the model state before assimilation. This investigation was performed on both $\text{HYCOM}_{\text{SLA}}$ and $\text{HYCOM}_{\text{SLA+SST}}$.

In order to expand on the increment analysis results, correlations between the model SSTs and observational sea surface heights (SSH) for a location (31°S, 16°E), where there are many cloud-free days and increments are substantial, are investigated. The MODIS SST and satellite altimetry SSH relationship for the same locations will provide a reference

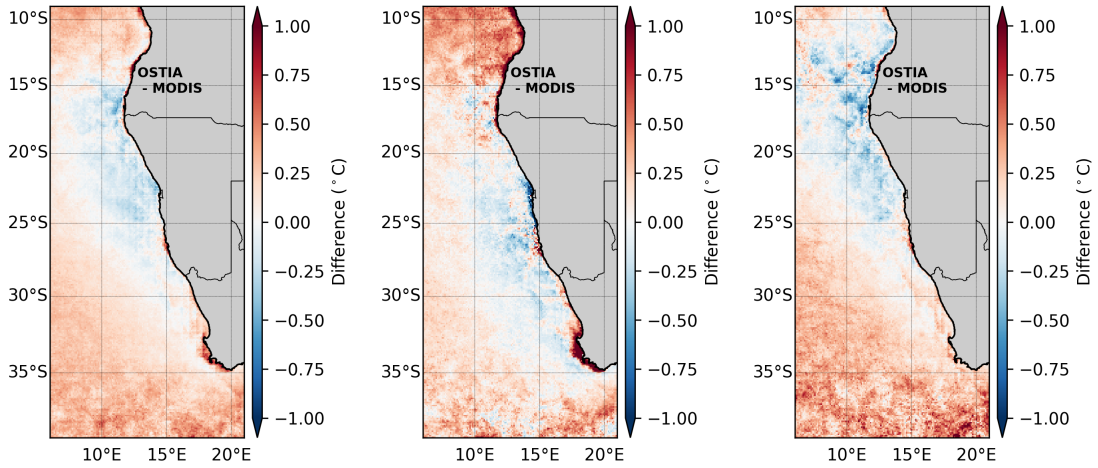

(a) 2-year mean. **(b)** Summer (JFM) mean. **(c)** Winter (JJA) mean.

Figure 3.2: Differences in mean SSTs between OSTIA and MODIS. Red (blue) shades indicate a warm (cold) bias in OSTIA.

of the expected relationship between SST and SSH for the location selected.

The satellite altimetry SSH used to evaluate the correlations is obtained from the level 4 sea surface topography product from CMEMS, previously distributed by Aviso+. It incorporates observations from all available altimeter missions interpolated to a horizontal grid with a resolution of 1/4°(∼25 km).

Chapter 4

Results and discussion

4.1 Mean state and variability

The 2-year mean SSTs for the models and satellite products are shown in Figure 4.1. Each of the models exhibit the colder band of water along the coast indicative of upwelling and in agreement with literature (Shannon 1985; Demarcq et al. 2003). The models also show an increase in temperature towards the north, where the influence of warmer Angola current waters are observed (Mohrholz et al. 2004; John et al. 2004) and as one moves out of the region of active coastal upwelling, warmer waters are seen in the south where the Agulhas Leakage enters the BUS (de Ruijter et al. 1999). Though something could be said for the ABFZ and the waters in the very north of the model domain, they are affected by heavy cloud cover (see Figure 3.1) and model boundary errors respectively, so they will only be discussed tentatively.

The upwelling extent of the three models vary slightly. $\text{HYCOM}_{\text{FREE}}$ and $\text{HYCOM}_{\text{SLA}}$ display a northern limit in the cool (16–18°C) SST at Walvis Bay (24°S) in the mean SSTs. $\text{HYCOM}_{\text{SLA+SST}}$ is in better agreement with the reference MODIS SSTs, displaying a cool temperature extent northwards of 20°S. The offshore extent of these waters is also underrepresented, but $\text{HYCOM}_{\text{SLA+SST}}$ is in best agreement with reference SSTs showing cooler temperatures reaching further offshore. The colder (14–16°C) waters close to the coast, as seen in the reference SSTs are diminished in all model runs. $\text{HYCOM}_{\text{SLA}}$, with the worst representation of the coastal upwelling extent has almost no waters in the 14–16°C temperature range. While $\text{HYCOM}_{\text{FREE}}$ and $\text{HYCOM}_{\text{SLA+SST}}$ fair well in their representation of these colder waters in the northern Benguela coastline, they are lacking in the southern region, particularly from the Cape Peninsula to St Helena Bay (32–33°S).

A potential reason for the reduced offshore extent of upwelled water in the models is that the winds at the coast are not properly resolved in the ERA-interim wind forcing. The reduced upwelling in the models suggests that the upwelling winds close to the coast are weaker than in reality, suggesting that ERA-interim possibly overestimates the wind speed drop-off from the open ocean to the coast. Upwelling studies using regional ocean models (Capet et al. 2004; Jacox and Edwards 2012) have shown that the upwelling response is susceptible to the wind stress drop-off near the coast, where the structure and dynamical control of the drop-off is an unresolved issue (Capet et al. 2004; Jin et al. 2009).

Concerning the warm Agulhas influence in the south, the satellite products suggest

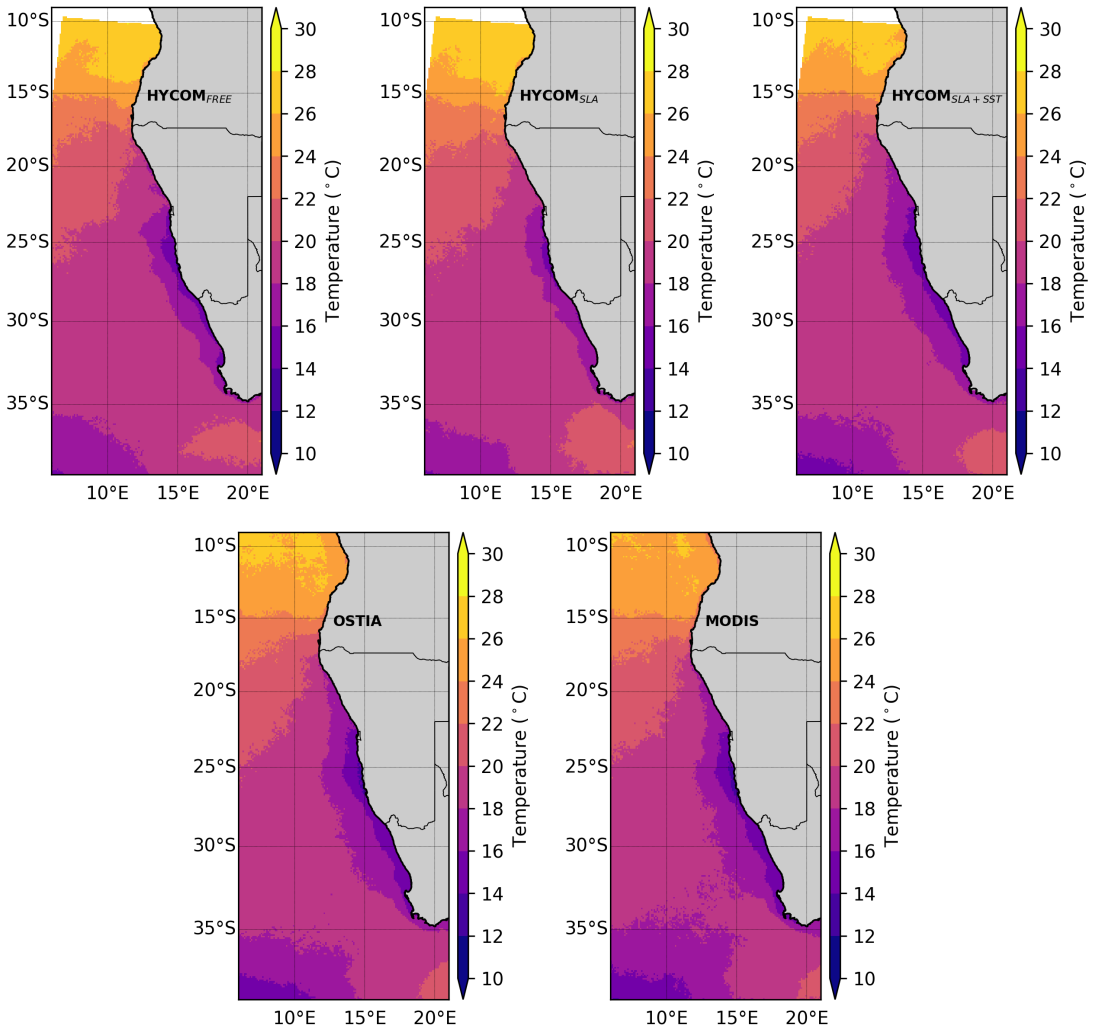

Figure 4.1: 2-year mean SSTs.

a much reduced impact in comparison to the models. This is visible in the warm (20–22°C) waters from the Agulhas retroflection near 37.5°S, 20°E that have an exaggerated westward/north-westward extent in the models compared to MODIS and OSTIA. This is likely due to the too regular and consistent passage of eddies from the Agulhas retroflection into the South Atlantic, a bias evident in HYCOM and many other ocean models of the region (Backeberg et al. 2014). This bias is also evident in the comparison of waters of temperature 18–20°C which are narrower in the MODIS product at ~32–35°S compared to the models. HYCOM$_{\mathrm{SLA+SST}}$ best resembles the reference data and assimilation of SLA only seems to worsen the estimate of the warmer waters associated with the passage of eddies into the South Atlantic.

Also captured in the model is the Subtropical Front (Deacon 1982) represented by the cool water (14–18°C) in the south-western corner of the study domain. This colder water is best represented in HYCOM$_{\mathrm{SLA+SST}}$, although it is still relatively diminished when compared to MODIS. HYCOM$_{\mathrm{FREE}}$ and HYCOM$_{\mathrm{SLA}}$ display a similar spread of SSTs in this region and are less representative of the observations.

Figure 4.2 indicates that the assimilation of along-track SLA does not improve the

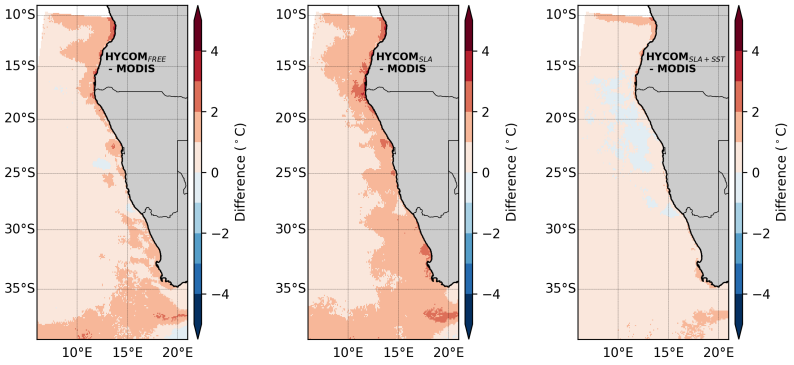

(a) Difference for 2008–2009.

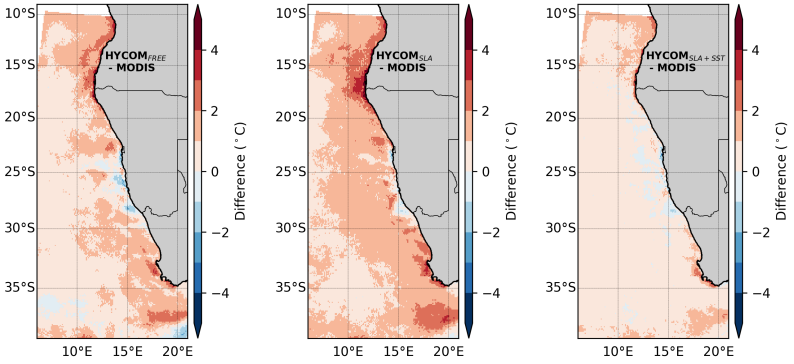

(b) Difference for summer months (JFM), 2008–2009.

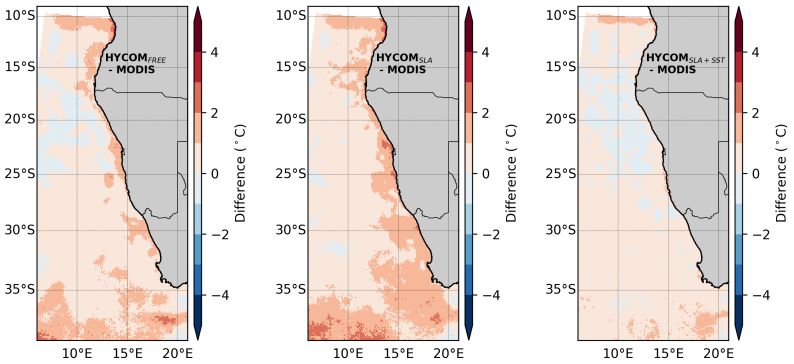

(c) Difference for winter months (JJA), 2008–2009.

Figure 4.2: Difference between HYCOM SST means and MODIS. Red shades indicate a warm bias in the models and blue shades indicate a cold bias in the models.

representation of SSTs in the BUS. Before assimilation, $\text{HYCOM}_{\text{FREE}}$ shows a clear warm bias (0–2°C) in the BUS compared to MODIS. The assimilation of along-track SLA degrades the SSTs along the coast and increases the warm bias (1–2°C) and its seaward extent. The introduction of OSTIA SST in the assimilation reduces the warm SST bias (0–1°C) in $\text{HYCOM}_{\text{FREE}}$ and $\text{HYCOM}_{\text{SLA}}$ compared to MODIS. While a warm bias is still present, it is much improved (<1°C) over the 1–2°C bias of $\text{HYCOM}_{\text{SLA}}$.

$\text{HYCOM}_{\text{FREE}}$ exhibits a warm bias (1–2°C) in the northern Benguela (∼17.5–25°S). This bias could be ascribed to missing Kelvin wave dynamics in the model due to them being absent in boundary conditions. This warm bias is also reflected in the $\text{HYCOM}_{\text{SLA}}$ output except that the bias is worsened. The areas of warm bias in the north, however,

are heavily affected by cloud cover over the study period (see Figure 3.1) and therefore it is difficult to make inferences about dynamical processes. Warm biases in the southern Benguela of both $\text{HYCOM}_{\text{FREE}}$ and $\text{HYCOM}_{\text{SLA}}$ could be due to an exaggerated wind stress drop-off (Jin et al. 2009) in ERA-interim wind forcing, as mentioned previously. There is a larger region along the coast at ∼25–29°S, in the vicinity of the Lüderitz cell, where $\text{HYCOM}_{\text{FREE}}$ shows minimal bias (0–1°C), suggesting that the free-running model is able to accurately represent features in this zone.

The basin scale HYCOM that the regional HYCOM is nested in (George et al. 2010) does not capture equatorially-forced Kelvin waves and so their effects are not transmitted to the nested HYCOM at the model boundaries. These coastally trapped waves propagate eastwards along the equator then polewards once reaching the coast, displacing the thermocline shallower(deeper) at each crest(trough) as they pass. This occasionally results in warm waters being upwelled instead of the usual cold waters from depth. Bachèlery et al. (2016) investigated the impact of local and remote forcing on variability in the south-east Atlantic. Remote forcing, as opposed to local forcing, was found to be more responsible for interannual variability. Kelvin waves were also observed propagating as far south as 26°S and caused ±2°C changes in temperatures below the thermocline. The fact that Kelvin waves are potentially resolved in the along-track SLA product assimilated into HYCOM, while their dynamics are absent from $\text{HYCOM}_{\text{FREE}}$ from which the static ensemble for the EnOI is derived, suggests that the assimilation of along-track SLA updates the analysis incorrectly. This potentially contributes to the warm bias in $\text{HYCOM}_{\text{SLA}}$ in the northern BUS in Figure 4.2a, though this contribution may be insignificant. Furthermore, the true impact of any Kelvin waves captured in the assimilated SLA on the model is unknown. Likewise, any influence of Kelvin waves on OSTIA and MODIS SSTs is also unestablished.

A large, offshore cool bias (-1–0°C) manifests in $\text{HYCOM}_{\text{SLA+SST}}$ at 15–25°S. The manifestation of the cooler regions in $\text{HYCOM}_{\text{SLA+SST}}$ may be due to similar, though more widespread, cool regions in the assimilated OSTIA SST as seen in Figure 3.2.

Seasonal differences (Figures 4.2b & 4.2c) indicate that biases are worse in the summer months for $\text{HYCOM}_{\text{FREE}}$ and $\text{HYCOM}_{\text{SLA}}$. This suggests that biases in the southern Benguela are associated with seasonal upwelling, but in the north, where upwelling is perennial, other drivers could be responsible for the bias, such as boundary conditions.

It is worth pointing out that the differences between $\text{HYCOM}_{\text{FREE}}$ and MODIS are of concern. The free-running model is the foundation of the static ensemble used to generate the error covariance matrices used in the assimilation process. Therefore, any errors and/or biases in the foundational $\text{HYCOM}_{\text{FREE}}$ model will propagate into the assimilated models affecting the forecast skill.

Standard deviations (Figure 4.3) of the models and remotely sensed data give an indication of the regional variability in SST. MODIS SSTs would suggest that there are two large areas of minimal (1–1.5°C) temperature variability over the period 2008–2009: from Cape Agulhas (35°S) nothwards along the coast to offshore of Cape Columbine (33°S); and the Lüderitz cell region (27°S). The Lüderitz cell is a perennial upwelling feature producing cold surface waters throughout the year (Lutjeharms and Meeuwis 1987), so the

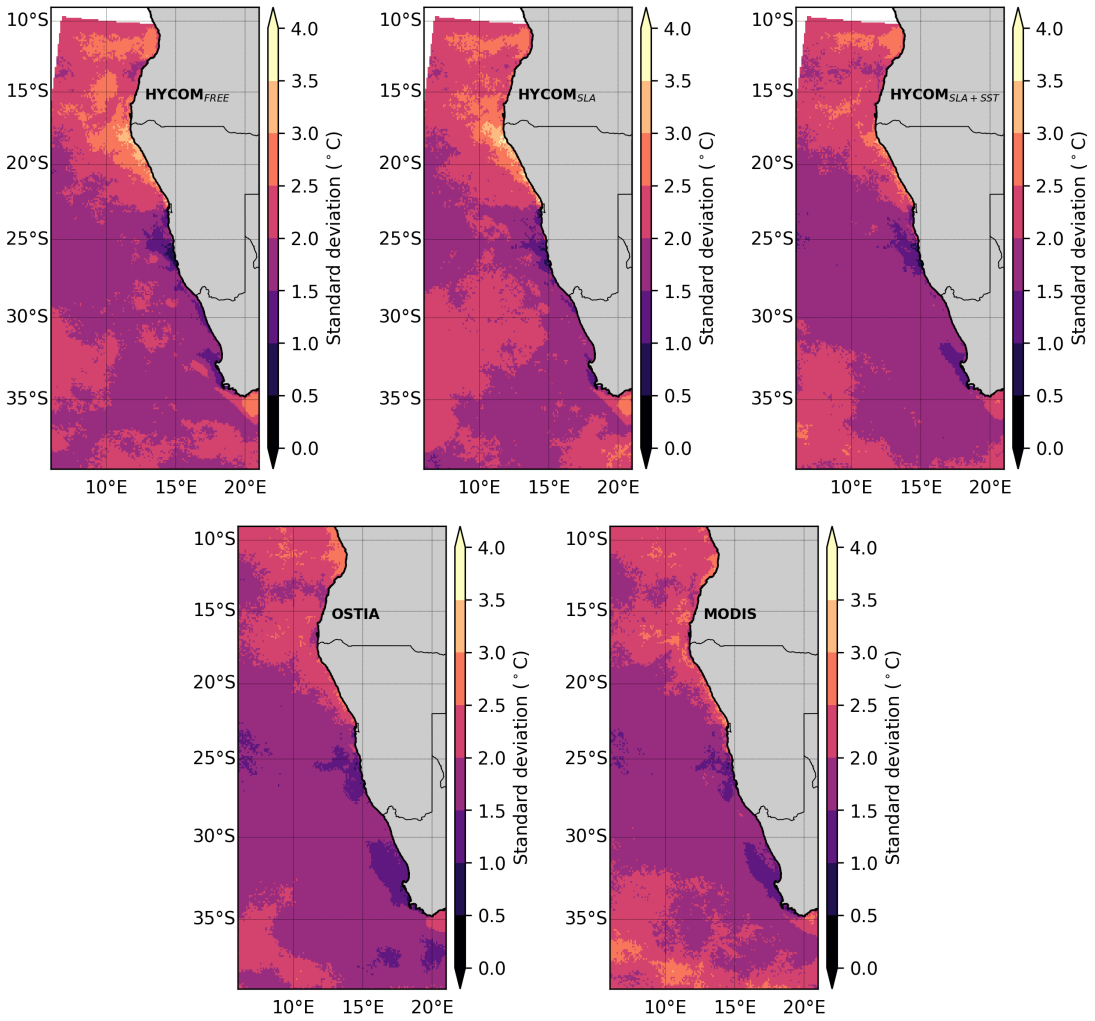

Figure 4.3: 2-year SST standard deviations.

reduced variability in the observations is expected. However, insolation is more likely to be responsible for the low variability at the Cape Peninsula upwelling cell (34°S) (Hardman-Mountford et al. 2003; Weeks et al. 2006; Demarcq et al. 2007). In the austral summer, surface waters are warmer due to solar insolation but upwelling around the Cape Peninsula upwelling cell results in colder surface waters at the coast. In winter, surface waters are cooler due to reduced insolation and upwelling at the Cape Peninsula is relaxed, resulting in surface waters that are similar in temperature to cooler offshore waters. The cooler winter waters at the Cape Peninsula upwelling cell during conditions of relaxed upwelling are similar in temperature to upwelled waters in summer, resulting in a reduced variance in temperatures and minimal variability.

Offshore variability in MODIS from 20–31°S is fairly uniform at 1.5–2°C with increased variability south of this latitude. Closer to shore, in the region of the Agulhas Leakage past the Cape Peninsula, this same pattern of 1.5–2°C variability is observed, pointing to a constant influence of warm Agulhas water entering the BUS.

HYCOM$_{\text{FREE}}$ also displays lowest variability (1–1.5°C) at the two main areas seen in MODIS, the Cape Agulhas and Cape Columbine regions, though to a lesser extent.

$HYCOM_{FREE}$ also shows increased variability (2–2.5°C) offshore compared to MODIS and reduced variability south-west of the Cape Peninsula, towards the Subtropical Front.

$HYCOM_{SLA}$ is much like $HYCOM_{FREE}$ in that it shows least variability at the Cape Agulhas-Columbine (∼33–35°S) region and at the Lüderitz cell. The variability at the former is, however, much reduced compared to both MODIS and $HYCOM_{FREE}$. More variability is present closer to shore (2–2.5°C at 26–35°S 10–14°E) compared to reference observations.

$HYCOM_{SLA+SST}$ SST variability compared to reference observations suggests that it once again outperforms both $HYCOM_{FREE}$ and $HYCOM_{SLA}$. The low variability in the Cape Peninsula area best matches the observations. Variability between the coast and the Subtropical Front is more uniform at 1.5–2°C and is constant, spanning a wide band in a north-westward to south-westward orientation from ∼18–36°S. Some increased variability in the observations are not captured south-west of Cape Peninsula at the Subtropical Front in $HYCOM_{SLA+SST}$, though. However, none of the models nor OSTIA capture the variability of SSTs at the Subtropical Front that MODIS does. OSTIA matches fairly well with MODIS, except that it exhibits more variability along the coast at and just above St Helena Bay (∼32–33°S). OSTIA also displays a reduced variability south of Cape Peninsula.

Examining the mean state and variability of the model SSTs has revealed a strong agreement between $HYCOM_{SLA+SST}$ and MODIS observations with warm biases evident in $HYCOM_{FREE}$ and $HYCOM_{SLA}$. Sub-optimal wind forcing is hypothesised to contribute to majority of the error with boundary conditions having an uncertain but potentially insignificant contribution.. In §4.2 an increment analysis is performed to better understand the impact that the assimilation of along-track SLA and OSTIA SSTs have on the model solution.

4.2 Increment analysis

To better understand the effects of assimilation on modelled variables, an increment analysis is performed for $HYCOM_{SLA}$ and $HYCOM_{SLA+SST}$. Increments are the adjustments made to variables during the assimilation cycle. Increments can be calculated for each variable by subtracting the forecast for assimilation day from the new analysis at assimilation day, resulting in increments brought about by the assimilation for the modelled variables.

Figure 4.4a shows the SSH increments for both assimilated model runs. Both $HYCOM_{SLA}$ and $HYCOM_{SLA+SST}$ show a net increase in SSH along the coast. SSH increments along the coast are in the range of ∼0–0.05 m. Seasonal signals in the increments follow the same pattern as the seasonal SST biases: increments are more severe in summer and less so in winter (see Appendix A) suggesting $HYCOM_{FREE}$ is more accurate in winter throughout the Benguela. SSH increments are slightly higher (by approximately 0.025 m) for $HYCOM_{SLA+SST}$. With $HYCOM_{SLA}$ having the largest warm bias of the models, it would suggest that, looking at SSH increments alone, $HYCOM_{SLA+SST}$ should also have a large warm SST bias. However, when examining SST increments (Figure 4.4b) it becomes clear that assimilating SSTs negates the warm bias created by the SLA assimilation.

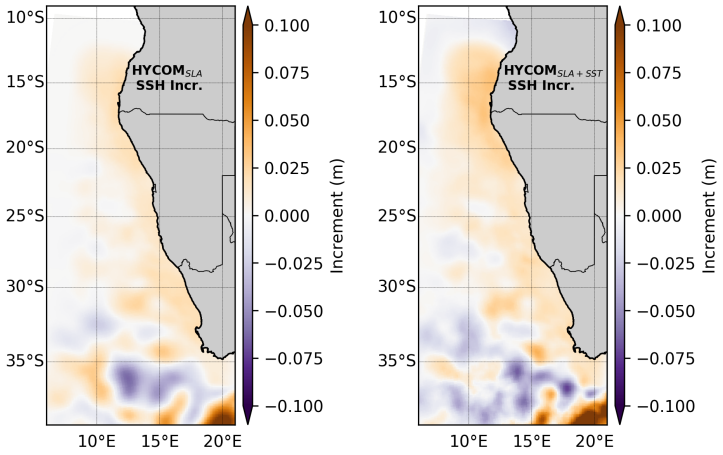

(a) SSH increments.

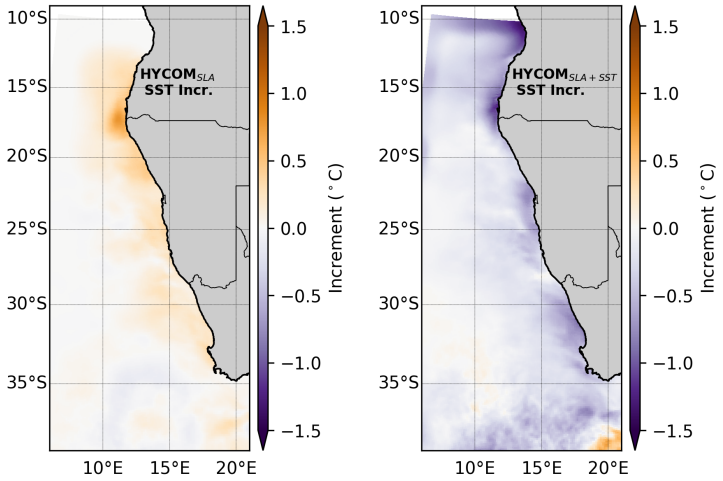

(b) SST increments.

Figure 4.4: Increments in **(a)** SSH and **(b)** SST for $\text{HYCOM}_{\text{SLA}}$ and $\text{HYCOM}_{\text{SLA+SST}}$ for the entire modelled period, 2008–2009.

Figure 4.4 suggests, when looking at the SST increments for $\text{HYCOM}_{\text{SLA}}$ and $\text{HYCOM}_{\text{SLA+SST}}$, that the increased SSH caused by the assimilation results in an increased SST. For $\text{HYCOM}_{\text{SLA+SST}}$, the SST increments are dramatically contrasting to that of $\text{HYCOM}_{\text{SLA}}$. There is a large negative increment (approximately -0.75–0°C). This suggests that the increased SST caused by increased SSH associated with SLA assimilation is corrected for by assimilating SST.

This close relationship between SSH and SST, where an increased SSH results in increased SST during assimilation of SLAs, is due to the SSH-SST relationship in the static ensemble, created using $\text{HYCOM}_{\text{FREE}}$. Using SSH from the daily CMEMS gridded product, the correlations between SSH and SST for each of the products is investigated. These correlations were examined at 31°S, 16°E, an area of significant increments where cloud cover was minimal so as to extract a large amount of data points. For each cloud free day at this location, SSH was extracted from the CMEMS product and the corresponding SST value was extracted from the models and satellite products. The correlation, R, between SSH and SST is calculated and shown in Figure 4.5.

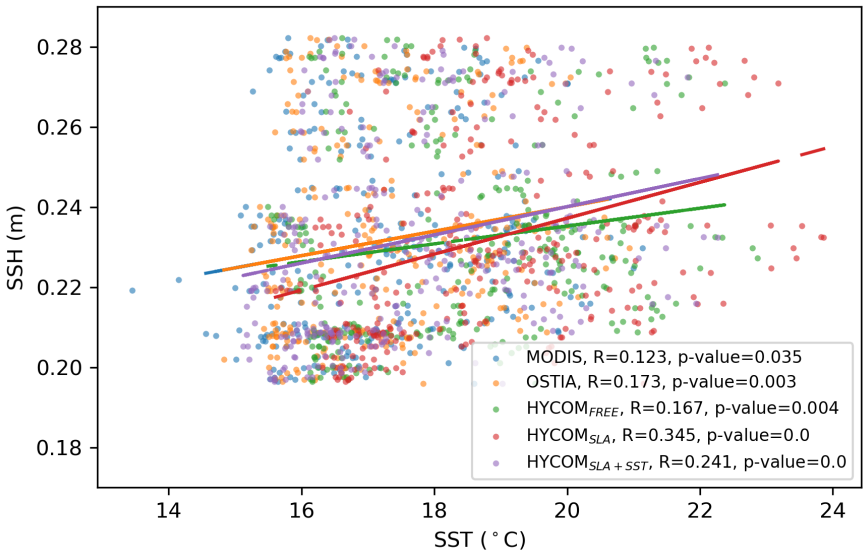

Figure 4.5: Correlation between SSH and SST for all HYCOM model runs, OSTIA and MODIS at 31°S, 16°E.

MODIS is considered as a reference of the relationship between SSH and SST (R = 0.123) that should ideally be observed in the other datasets. HYCOM$_{\text{FREE}}$ exhibits a slightly stronger SSH-SST relationship (R = 0.167). Hence, during the assimilation of SLA, a small increase in SSH results in a large increase in SST. This warm bias, which is also present in the static ensemble because it is constructed using HYCOM$_{\text{FREE}}$, is then exacerbated when assimilating along-track SLA. The incorrect SSH-SST relationship in HYCOM$_{\text{FREE}}$/the static ensemble then results in an erroneous SSH-SST relationship in HYCOM$_{\text{SLA}}$ (R = 0.345). HYCOM$_{\text{SLA}}$ bears a stronger correlation due to the prevalence of positive SSH increments at the location where the SSH-SST relationships were evaluated (see Figure 4.4a). Assimilating OSTIA SSTs improves the relationship (R = 0.241), but the HYCOM$_{\text{SLA+SST}}$ correlation can not be corrected to that of MODIS because the assimilated OSTIA SSTs also exhibit an incorrect relationship (R = 0.173) and because of the inherent limitations in HYCOM$_{\text{FREE}}$ and the static ensemble derived from it.

These results indicate that HYCOM$_{\text{FREE}}$ has an inherent misrepresentation of the SSH-SST relationship and assimilating along-track SLA therefore incorrectly adjusts SST for HYCOM$_{\text{SLA}}$. As an example, a positive SLA assimilation results in an increased SSH. The SSH-SST relationship in HYCOM$_{\text{FREE}}$ causes SST to increase in response. However, compared to the MODIS SSH-SST, the HYCOM$_{\text{FREE}}$ relationship causes too high an increase in SST. As suggested earlier (§3.1.2), the incorrect relationship in HYCOM$_{\text{FREE}}$ could be due to the effect of the global warming signal in the static ensemble, contributing to the correlation. Care must, however, be taken when interpreting the SSH-SST relationships as the incorporated level 4 CMEMS product uses an averaging window of ∼34 days, meaning upwelling events of a lesser duration are not captured. It is acknowledged that the SSH-SST relationships shown are not necessarily the truth.

Examining the increments for surface velocities provides insights into the impact of the

assimilation on circulation dynamics in the model. Figure 4.6a shows that the $\text{HYCOM}_{\text{SLA}}$ mean surface velocities in the BUS are in a north-westward direction, which is the expected response from the predominantly alongshore wind in the region responsible for the upwelling at the coast (Nelson and Hutchings 1983; Shannon 1985). The increments, however, are mostly in a south-eastward direction, in the opposite direction to the predominant flow. These increments therefore reduce the upwelling currents contributing to the warm bias evident in $\text{HYCOM}_{\text{SLA}}$.

$\text{HYCOM}_{\text{SLA+SST}}$ displays a very similar mean surface flow to $\text{HYCOM}_{\text{SLA}}$. The increments, however, would appear to be more severe although still in a direction that would suppress upwelling. This was also seen in the SSH increments (see Figure 4.4b). This would insinuate that the inclusion of OSTIA in the assimilation reduces the SSTs but does not increase the upwelling currents, suggesting that the SST product does not have a strong positive impact on the currents associated with the upwelling dynamics.

From the increments in surface velocities, results would suggest that while $\text{HYCOM}_{\text{SLA}}$ experiences reduced offshore flow, $\text{HYCOM}_{\text{SLA+SST}}$ exhibits the same changes and to a more severe degree. This implies that the improved SSTs seen in $\text{HYCOM}_{\text{SLA+SST}}$ are not due to an improved representation of upwelling dynamics, but rather they are only due to OSTIA's ability to reduce the SST bias in HYCOM during assimilation.

The increment analysis has revealed that assimilation of along-track SLA results in a positive SST increment culminating in a warm bias, but when also assimilating SST a negative SST increment results, significantly reducing the warm bias. The significant warm bias in $\text{HYCOM}_{\text{SLA}}$ is due to an incorrect relationship between SSH and SST in $\text{HYCOM}_{\text{FREE}}$ (small increases in SSH result in large increases in SST). The static ensemble, which determines the forecast error of the EnOI is derived from $\text{HYCOM}_{\text{FREE}}$ and therefore adversely affects the model solution in the assimilation of SLA. The SSH-SST relationship is improved in $\text{HYCOM}_{\text{SLA+SST}}$, but an incorrect SSH-SST relationship in the assimilated OSTIA SSTs (compared to MODIS), in addition to the biases in $\text{HYCOM}_{\text{FREE}}$ prevent a complete rectification of the error. Increments in surface velocities also suggest that assimilation of SLA and SST could be degrading the forecast by reducing the upwelling-favourable currents.

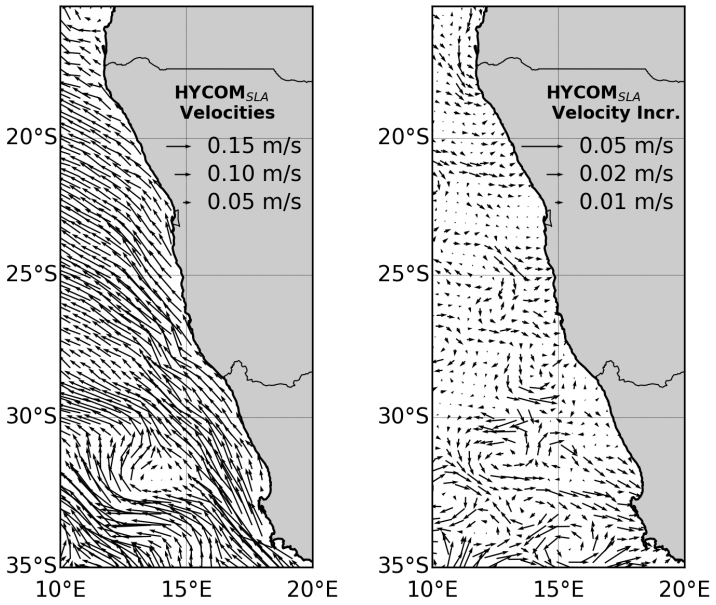

(a) HYCOM$_{\mathrm{SLA}}$.

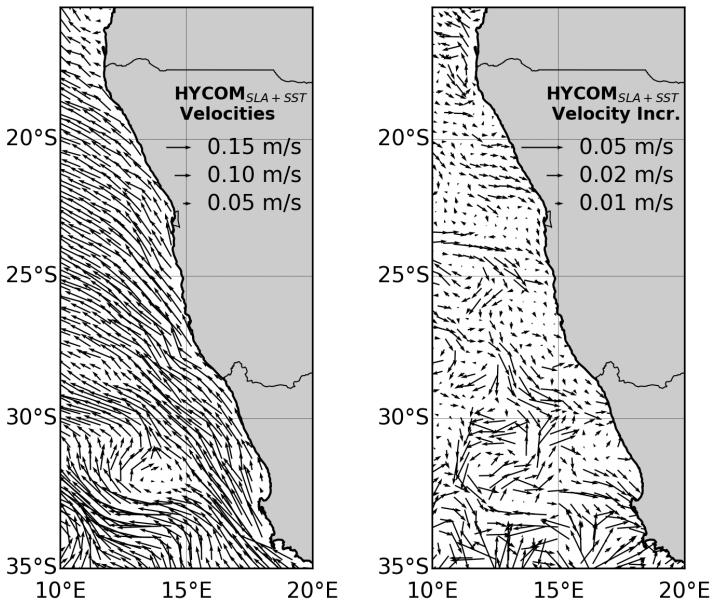

(b) HYCOM$_{\mathrm{SLA+SST}}$.

Figure 4.6: Mean surface velocities and surface velocity increments for **(a)** HYCOM$_{\mathrm{SLA}}$ and **(b)** HYCOM$_{\mathrm{SLA+SST}}$ for the entire modelled period, 2008–2009.

Chapter 5

Summary and conclusion

This study investigated the effects of assimilating SSTs and along-track SLAs, using the EnOI assimilation scheme, on forecasted upwelling dynamics in the Benguela Upwelling System using HYCOM. A regional HYCOM, nested in a basin-scale HYCOM, was utilised in three modes: (1.) free-running mode ($\text{HYCOM}_{\text{FREE}}$), (2.) assimilating CMEMS along-track SLAs ($\text{HYCOM}_{\text{SLA}}$) and (3.) assimilating along-track SLAs as well as OSTIA SSTs ($\text{HYCOM}_{\text{SLA+SST}}$). MODIS SSTs were then used as reference observations to evaluate the models' skill at representing and forecasting surface SSTs.

Comparing the assimilated OSTIA SSTs to the reference MODIS SSTs (Figure 3.2) revealed minor warm and cold biases in OSTIA. Warm biases of 0.25 to 0.75°C were apparent generally offshore and in the northern (10–15°S) and southern (35–40°S) regions of the study area. A constant cold bias of -0.50 to -0.25°C existed at the coast with a more southward (northward) location in the austral summer (winter).

Each of the models reproduced (Figure 4.1) the cool region of upwelling along the coast and the warmer waters at the Angola Current interface to the north, at the Aghulhas Current interface in the south and those further offshore. Variability, represented by SST standard deviations, also matched most large features of the region.

Compared to MODIS (Figure 4.2), $\text{HYCOM}_{\text{FREE}}$ exhibited a warm bias (1–2°C) in the comparisons to MODIS SSTs and showed a slight increase in SST variability. $\text{HYCOM}_{\text{SLA}}$ displayed more widespread, greater warm biases (1–3°C) and increased variability across the majority of the coastal region. $\text{HYCOM}_{\text{SLA+SST}}$ was much improved over its two counterparts, matching well with the reference observations.

An increment analysis was then performed to better understand the effects of assimilation on the modelled variables (Figure 4.4). Increments in SSH for both assimilated models were very similar in distribution and magnitude (0.025–0.050 m), but increments were slightly intensified for $\text{HYCOM}_{\text{SLA+SST}}$. SST increments revealed a slight warming (0.25–0.075°C) in $\text{HYCOM}_{\text{SLA}}$ and a large cooling (-0.25 to -1.00°C) in $\text{HYCOM}_{\text{SLA+SST}}$. This suggests that any warming brought about by the assimilation of SLAs is negated by the SST assimilation.

Theorising that the increased SSTs in $\text{HYCOM}_{\text{SLA}}$ are a response to increased SSH caused by SLA assimilation, the SSH-SST relationship was investigated for each model and compared to satellite products (Figure 4.5). Using MODIS as a reference correlation

(R = 0.123), $HYCOM_{FREE}$ displayed an erroneous correlation (R = 0.167) in comparison. As a result of the incorrect SSH-SST relationship in $HYCOM_{FREE}$, the resulting SSH-SST relationship in $HYCOM_{SLA}$ is incorrectly stronger (R = 0.345) than the satellite observed SSH-SST relationship. This is corrected for during the assimilation of SST in $HYCOM_{SLA+SST}$, which brings the SSH-SST relationship (R = 0.241) closer to observations, but it can not fully correct it because of inherent weaknesses in $HYCOM_{FREE}$ from which the static ensemble for the EnOI is derived and an incorrect SSH-SST relationship in the assimilated SSTs (R = 0.173). However, the level 4 SSH dataset used for evaluation of this relationship does not resolve upwelling dynamics at timescales less than ∼34 days, therefore the relationships may not represent the truth faithfully.

A look at the increments in the surface velocities (Figure 4.6) reveals that the assimilation is reducing the upwelling-favourable currents, thereby reducing upwelling, accounting for the warm bias in the BUS. This impact is seen in both $HYCOM_{SLA}$ and $HYCOM_{SLA+SST}$, but the reduction in upwelling favourable currents is more severe in $HYCOM_{SLA+SST}$. Therefore, although assimilating SSTs allows for a reduction of surface temperature bias, it suggests it is unable to correct the unfavourable upwelling dynamics introduced by the SLA assimilation.

The EnOI assimilation scheme relies on a static ensemble from which error covariances are generated for each assimilation cycle. $HYCOM_{FREE}$, the model used to generate the static ensemble, contains a bias (Figure 4.2) and an incorrect SSH-SST relationship. Hence, the static ensemble contains both a bias and incorrect dynamics, which are translated to the model forecast during the assimilation of both SLA and SST. The effects of global warming could also be present in the ensemble, but its effect has not been quantified.

Warm coastal biases observed in HYCOM are hypothesised to potentially be due to errors in the ERA-interim wind forcing used in the model. A possible overestimation of wind speed drop-off towards the coast from offshore results in weaker winds at the shore and reduced upwelling. The resultant warm SST bias is corrected for in $HYCOM_{SLA+SST}$ due to the assimilation of OSTIA SSTs.

Furthermore, the warm biases in $HYCOM_{SLA}$ are increased due to the incorrect SSH-SST relationship in $HYCOM_{FREE}$. The bias in $HYCOM_{FREE}$ in the northern Benguela (∼15–26°S) could be associated with the absence of equatorially-forced Kelvin waves, propagating southward along the coastline and displacing the thermocline. The basin-scale HYCOM does not include the Equator and the climatological boundary conditions of the outer HYCOM do not resolve Kelvin waves and therefore these signals are not transmitted to the nested HYCOM at the model boundaries. However, Kelvin wave signals are resolved in the assimilated along-track SLA product, but due to the incorrect SST response in the static ensemble (Figure 4.5) they could be causing a warm response in the regional model. Yet, due to the nature of Kelvin waves, their influence on the SST bias could be insignificant.

$HYCOM_{SLA+SST}$ shows improved modelled SSTs (Figure 4.2). Overall the bias is reduced, but an area of cool bias persists, which is potentially the result of a cool bias in the assimilated OSTIA SSTs (Figure 3.2). OSTIA shows differences of up to ±1°C compared

to MODIS and is a considerably smoothed SST product designed for assimilation into numerical weather prediction models. Its use in this assimilation study vastly improved surface $\text{HYCOM}_{\text{SLA+SST}}$ SSTs, but its difference to MODIS suggests it might not be optimal for this specific application. The forecast SSTs could be improved by assimilating a more suitable SST product.

Although assimilating along-track SLAs degraded forecast SSTs and assimilating SSTs reduced the bias, this study indicates that most of the error, in particular the bias, is associated with $\text{HYCOM}_{\text{FREE}}$ which is unable to model the correct SSH-SST relationship in the BUS. Assimilating observations has a knock-on effect on other variables as determined by the static ensemble, some of which may not be desirable. Future studies should work towards optimising $\text{HYCOM}_{\text{FREE}}$ for simulating the upwelling dynamics in the BUS. This may include increasing the horizontal and vertical resolution of the model, and increasing the ratio of sigma to isopycnal coordinates used. The effects of wind forcing, particularly the wind drop-off towards the coast, and improving the model boundaries should also be investigated. Particularly, including equatorially-forced Kelvin waves in the boundary conditions may have a significant impact on the upwelling dynamics of the northern BUS.

Chapter 6

Bibliography

Antonov, J., Locarnini, R., Boyer, T., Mishonov, A., and HE, G. (2006). *World Ocean Atlas 2005, Volume 1: Salinity*. U.S. Government Printing Office, Washington. NOAA Atlas NESDIS 61.

Bachèlery, M.-L., Illig, S., and Dadou, I. (2016). Interannual variability in the South-East Atlantic Ocean, focusing on the Benguela Upwelling System: Remote versus local forcing. *Journal of Geophysical Research: Oceans*, 121(1):284–310.

Backeberg, B., Bertino, L., and Johannessen, J. (2009). Evaluating two numerical advection schemes in HYCOM for eddy-resolving modelling of the Agulhas Current. *Ocean Sci*, 5:173–190.

Backeberg, B. and Reason, C. (2010). A connection between the South Equatorial Current north of Madagascar and Mozambique Channel eddies. *Geophysical Research Letters*, 37(4).

Backeberg, B. C., Counillon, F., Johannessen, J. A., and Pujol, M.-I. (2014). Assimilating along-track SLA data using the EnOI in an eddy resolving model of the Agulhas system. *Ocean Dynamics*, 64(8):1121–1136.

Backeberg, B. C., Johannessen, J. A., Bertino, L., and Reason, C. (2008). The greater Agulhas Current system: An integrated study of its mesoscale variability. *Journal of Operational Oceanography*, 1(1):29–44.

Bang, N. (1971). The southern Benguela Current region in February, 1966: Part II. Bathythermography and air-sea interactions. In *Deep Sea Research and Oceanographic Abstracts*, volume 18, pages 209–224. Elsevier.

Bang, N. and Andrews, W. (1974). Direct current measurements of a shelf-edge frontal jet in the southern Benguela system. *Journal of Marine Research*, 32:405–417.

Batteen, M. L., Martinho, A. S., Miller, H. A., and McClean, J. L. (2007). A process-oriented modelling study of the coastal Canary and Iberian Current system. *Ocean Modelling*, 18(1):1–36.

Belmadani, A., Echevin, V., Dewitte, B., and Colas, F. (2012). Equatorially forced intraseasonal propagations along the Peru-Chile coast and their relation with the nearshore eddy activity in 1992–2000: A modeling study. *Journal of Geophysical Research: Oceans*, 117(C4).

Bentsen, M., Evensen, G., Drange, H., and Jenkins, A. (1999). Coordinate transformation on a sphere using conformal mapping. *Monthly Weather Review*, 127(12):2733–2740.

Berge, T., Aminzadeh, F., de Groot, P., and Oldenziel, T. (2002). Seismic inversion successfully predicts reservoir, porosity, and gas content in Ibhubesi Field, Orange Basin, South Africa. *The Leading Edge*, 21(4):338–348.

Bertino, L., Evensen, G., and Wackernagel, H. (2003). Sequential data assimilation techniques in oceanography. *International Statistical Review*, 71(2):223–241.

Bianchi, G., Hamukuaya, H., and Alvheim, O. (2001). On the dynamics of demersal fish assemblages off Namibia in the 1990s. *South African Journal of Marine Science*, 23(1):419–428.

Blanke, B., Roy, C., Penven, P., Speich, S., McWilliams, J., and Nelson, G. (2002). Linking wind and interannual upwelling variability in a regional model of the southern Benguela. *Geophysical Research Letters*, 29(24).

Blanke, B., Speich, S., Bentamy, A., Roy, C., and Sow, B. (2005). Modeling the structure and variability of the southern Benguela upwelling using QuikSCAT wind forcing. *Journal of Geophysical Research: Oceans*, 110(C7).

Bleck, R. (2002). An oceanic general circulation model framed in hybrid isopycnic-Cartesian coordinates. *Ocean modelling*, 4(1):55–88.

Bleck, R., Rooth, C., Hu, D., and Smith, L. T. (1992). Salinity-driven thermocline transients in a wind-and thermohaline-forced isopycnic coordinate model of the North Atlantic. *Journal of Physical Oceanography*, 22(12):1486–1505.

Boyd, A. and Nelson, G. (1998). Variability of the Benguela current off the cape Peninsula, South Africa. *African Journal of Marine Science*, 19.

Boyer, D., Cole, J., and Bartholomae, C. (2000). Southwestern Africa: Northern Benguela Current region. *Marine Pollution Bulletin*, 41(1):123–140.

Britz, P. and Venter, S. (2016). Aquaculture Review: South Africa. *World Aquaculture*, pages 20–28.

Broquet, G., Edwards, C., Moore, A., Powell, B., Veneziani, M., and Doyle, J. (2009). Application of 4D-Variational data assimilation to the California Current System. *Dynamics of Atmospheres and Oceans*, 48(1-3):69–92.

Broquet, G., Moore, A., Arango, H., and Edwards, C. (2011). Corrections to ocean surface forcing in the California Current System using 4D variational data assimilation. *Ocean Modelling*, 36(1-2):116–132.

Browning, G. and Kreiss, H.-O. (1982). Initialization of the shallow water equations with open boundaries by the bounded derivative method. *Tellus*, 34(4):334–351.

Browning, G. and Kreiss, H.-O. (1986). Scaling and computation of smooth atmospheric motions. *Tellus A*, 38(4):295–313.

Byrne, D. and McClean, J. (2008). Sea level anomaly signals in the Agulhas Current region. *Geophysical Research Letters*, 35(13).

Capet, X., Marchesiello, P., and McWilliams, J. (2004). Upwelling response to coastal wind profiles. *Geophysical Research Letters*, 31(13).

Chao, Y., Li, Z., Farrara, J., McWilliams, J. C., Bellingham, J., Capet, X., Chavez, F., Choi, J.-K., Davis, R., Doyle, J., et al. (2009). Development, implementation and evaluation of a data-assimilative ocean forecasting system off the central California coast.

Deep Sea Research Part II: Topical Studies in Oceanography, 56(3-5):100–126.

Chassignet, E. P., Hurlburt, H. E., Smedstad, O. M., Halliwell, G. R., Hogan, P. J., Wallcraft, A. J., Baraille, R., and Bleck, R. (2007). The HYCOM (hybrid coordinate ocean model) data assimilative system. *Journal of Marine Systems*, 65(1):60–83.

Chelton, D. B., Deszoeke, R. A., Schlax, M. G., El Naggar, K., and Siwertz, N. (1998). Geographical variability of the first baroclinic Rossby radius of deformation. *Journal of Physical Oceanography*, 28(3):433–460.

Colberg, F. and Reason, C. (2006). A model study of the Angola Benguela Frontal Zone: Sensitivity to atmospheric forcing. *Geophysical research letters*, 33(19).

Combes, V., Di Lorenzo, E., Gómez, F., Hormazabal, S., Strub, T. P., and Putrasahan, D. (2009). Modeling interannual and decadal variability in the Humboldt current upwelling system. *Journal of Physical Oceanography*.

Counillon, F. and Bertino, L. (2009). Ensemble Optimal Interpolation: multivariate properties in the Gulf of Mexico. *Tellus A*, 61(2):296–308.

Crosman, E. T. and Horel, J. D. (2009). MODIS-derived surface temperature of the Great Salt Lake. *Remote Sensing of Environment*, 113(1):73–81.

de Ruijter, W., Biastoch, A., Drijfhout, S., Lutjeharms, J., Matano, R., Pichevin, T., Leeuwen, P. v., and Weijer, W. (1999). Indian-Atlantic interocean exchange: Dynamics, estimation and impact. *Journal of Geophysical Research: Oceans*, 104(C9):20885–20910.

Deacon, G. (1982). Physical and biological zonation in the Southern Ocean. *Deep Sea Research Part A. Oceanographic Research Papers*, 29(1):1–15.

Dee, D. P., Uppala, S., Simmons, A., Berrisford, P., Poli, P., Kobayashi, S., Andrae, U., Balmaseda, M., Balsamo, G., Bauer, P., Bechtold, P., Beljaars, A., van de Berg, L., Bidlot, J., Bormann, N., Delsol, C., Dragani, R., Fuentes, M., Geer, A., Haimberger, L., Healy, S., Hersbach, H., Hólm, E., Isaksen, L., Kållberg, P., Köhler, M., Matricardi, M., McNally, A., Monge-Sanz, B., Morcrette, J.-J., Park, B.-K., Peubey, C., de Rosnay, P., Tavolato, C., Thépaut, J.-N., and Vitart, F. (2011). The ERA-Interim reanalysis: Configuration and performance of the data assimilation system. *Quarterly Journal of the royal meteorological society*, 137(656):553–597.

Demarcq, H., Barlow, R., and Hutchings, L. (2007). Application of a chlorophyll index derived from satellite data to investigate the variability of phytoplankton in the Benguela ecosystem. *African Journal of Marine Science*, 29(2):271–282.

Demarcq, H., Barlow, R., and Shillington, F. (2003). Climatology and variability of sea surface temperature and surface chlorophyll in the Benguela and Agulhas ecosystems as observed by satellite imagery. *African Journal of Marine Science*, 25(1):363–372.

Department: Planning, Monitoring and Evaluation (2014). Operation Phakisa. http://www.operationphakisa.gov.za/operations/oel/pages/default.aspx (Visited: 6 August 2017).

Dibarboure, G., Pujol, M.-I., Briol, F., Traon, P. L., Larnicol, G., Picot, N., Mertz, F., and Ablain, M. (2011). Jason-2 in DUACS: Updated system description, first tandem results and impact on processing and products. *Marine Geodesy*, 34(3-4):214–241.

Donlon, C. J., Martin, M., Stark, J., Roberts-Jones, J., Fiedler, E., and Wimmer, W.

(2012). The operational sea surface temperature and sea ice analysis (OSTIA) system. *Remote Sensing of Environment*, 116:140–158.

Drange, H. and Simonsen, K. (1996). *Formulation of air-sea fluxes in the ESOP2 version of MICOM*. Nansen Environmental and Remote Sensing Center.

Ducet, N., Le Traon, P.-Y., and Reverdin, G. (2000). Global high-resolution mapping of ocean circulation from TOPEX/Poseidon and ERS-1 and-2. *Journal of Geophysical Research: Oceans*, 105(C8):19477–19498.

Dufois, F., Penven, P., Whittle, C. P., and Veitch, J. (2012). On the warm nearshore bias in Pathfinder monthly SST products over Eastern Boundary Upwelling Systems. *Ocean Modelling*, 47:113–118.

Echevin, V., Colas, F., Chaigneau, A., and Penven, P. (2011). Sensitivity of the Northern Humboldt Current System nearshore modeled circulation to initial and boundary conditions. *Journal of Geophysical Research: Oceans*, 116(C7).

Echevin, V., Goubanova, K., Belmadani, A., and Dewitte, B. (2012). Sensitivity of the Humboldt Current system to global warming: a downscaling experiment of the IPSL-CM4 model. *Climate Dynamics*, 38(3-4):761–774.

Escribano, R., Rosales, S. A., and Blanco, J. L. (2004). Understanding upwelling circulation off Antofagasta (northern Chile): a three-dimensional numerical-modeling approach. *Continental Shelf Research*, 24(1):37–53.

Evensen, G. (1994). Sequential data assimilation with a nonlinear quasi-geostrophic model using Monte Carlo methods to forecast error statistics. *Journal of Geophysical Research: Oceans*, 99(C5):10143–10162.

Evensen, G. (2003). The ensemble Kalman filter: Theoretical formulation and practical implementation. *Ocean dynamics*, 53(4):343–367.

Fennel, W., Junker, T., Schmidt, M., and Mohrholz, V. (2012). Response of the Benguela upwelling systems to spatial variations in the wind stress. *Continental Shelf Research*, 45:65–77.

FIH (2009). *Fishing Industry Handbook South Africa, Namibia and Moçambique*. George Warman Publications, Cape Town, 37 edition.

Fu, W., She, J., and Zhuang, S. (2011). Application of an Ensemble Optimal Interpolation in a North/Baltic Sea model: Assimilating temperature and salinity profiles. *Ocean Modelling*, 40(3):227–245.

Gaspari, G. and Cohn, S. E. (1999). Construction of correlation functions in two and three dimensions. *Quarterly Journal of the Royal Meteorological Society*, 125(554):723–757.

George, M., Bertino, L., Johannessen, O., and Samuelsen, A. (2010). Validation of a hybrid coordinate ocean model for the Indian Ocean. *Journal of Operational Oceanography*, 3(2):25–38.

Goodrum, G., Kidwell, K., and Winston, W. (2000). NOAA KLM user's guide. NOAA. Technical report, NOAA-NESDIS/NCDC, Suitland, Maryland, USA.

Gordon, A. L. and Bosley, K. T. (1991). Cyclonic gyre in the tropical South Atlantic. *Deep Sea Research Part A. Oceanographic Research Papers*, 38:S323–S343.

Griffies, S. M., Schmidt, M., and Herzfeld, M. (2009). Elements of mom4p1. *GFDL Ocean*

Group Technical Report, 6:377.

Griffiths, C. L., Van Sittert, L., Best, P., Brown, A., Clark, B., Cook, P., Crawford, R. J., David, J., Davies, B., Griffiths, M., Hutchings, K., Jerardino, A., Karenyi, N., Lamberth, S., Leslie, R., Melville-Smith, R., Tarr, R., and van der Lingen, C. J. (2005). Impacts of human activities on marine animal life in the Benguela: a historical overview. *Oceanogr. Mar. Biol. Annu. Rev.*, 42:303–392.

Hao, Y., Cui, T., Singh, V. P., Zhang, J., Yu, R., and Zhang, Z. (2017). Validation of MODIS Sea Surface Temperature Product in the Coastal Waters of the Yellow Sea. *IEEE Journal of Selected Topics in Applied Earth Observations and Remote Sensing*, 10(5):1667–1680.

Hardman-Mountford, N., Richardson, A., Agenbag, J., Hagen, E., Nykjaer, L., Shillington, F., and Villacastin, C. (2003). Ocean climate of the South East Atlantic observed from satellite data and wind models. *Progress in Oceanography*, 59(2-3):181–221.

Hill, A., Hickey, B., Shillington, F., Strub, P., Brink, K., Barton, E., and Thomas, A. (1998). Eastern boundary currents: a pan-regional review. In Robinson, A. and Brink, K., editors, *The Sea. Volume 11. The global coastal ocean. Regional studies and syntheses*, pages 29–68. John Wiley and Sons Ltd, New York.

Hutchings, L. (1992). Fish harvesting in a variable, productive environment—searching for rules or searching for exceptions? *South African Journal of Marine Science*, 12(1):297–318.

Hutchings, L., Van der Lingen, C., Shannon, L., Crawford, R., Verheye, H., Bartholomae, C., Van der Plas, A., Louw, D., Kreiner, A., Ostrowski, M., Fidel, Q., Barlow, R., Lamont, T., Coetzee, J., Shillington, F., Veitch, J., Currie, J., and Monteiro, P. (2009). The Benguela Current: An ecosystem of four components. *Progress in Oceanography*, 83(1):15–32.

Ikeda, M. and Emery, W. (1984). Satellite observations and modeling of meanders in the California Current system off Oregon and northern California. *Journal of Physical Oceanography*, 14(9):1434–1450.

Jacox, M. and Edwards, C. (2012). Upwelling source depth in the presence of nearshore wind stress curl. *Journal of Geophysical Research: Oceans*, 117(C5).

Jennings, S., Kaiser, M. J., and Reynolds, J. D. (2009). *Marine fisheries ecology*. Blackwell Publishing.

Jin, X., Dong, C., Kurian, J., McWilliams, J. C., Chelton, D. B., and Li, Z. (2009). SST–wind interaction in coastal upwelling: Oceanic simulation with empirical coupling. *Journal of Physical Oceanography*, 39(11):2957–2970.

John, H.-C., Mohrholz, V., Lutjeharms, J., Weeks, S., Cloete, R., Kreiner, A., and da Silva Neto, D. (2004). Oceanographic and faunistic structures across an Angola Current intrusion into northern Namibian waters. *Journal of marine systems*, 46(1):1–22.

Johnson, J. and Stevens, I. (2000). A fine resolution model of the eastern North Atlantic between the Azores, the Canary Islands and the Gibraltar Strait. *Deep Sea Research Part I: Oceanographic Research Papers*, 47(5):875–899.

Junker, T., Schmidt, M., and Mohrholz, V. (2015). The relation of wind stress curl and meridional transport in the Benguela upwelling system. *Journal of Marine Systems*, 143:1–6.

Jury, M., MacArthur, C., and Brundrit, G. (1990). Pulsing of the Benguela upwelling region: large-scale atmospheric controls. *South African Journal of Marine Science*, 9(1):27–41.

Kara, A. B., Rochford, P. A., and Hurlburt, H. E. (2000). Efficient and accurate bulk parameterizations of air–sea fluxes for use in general circulation models. *Journal of Atmospheric and Oceanic Technology*, 17(10):1421–1438.

Koné, n. V., Machu, E., Penven, P., Andersen, V., Garçon, V., Fréon, P., and Demarcq, H. (2005). Modeling the primary and secondary productions of the southern Benguela upwelling system: A comparative study through two biogeochemical models. *Global Biogeochemical Cycles*, 19(4).

Koseki, S., Keenlyside, N., Demissie, T., Toniazzo, T., Counillon, F., Bethke, I., Ilicak, M., and Shen, M.-L. (2018). Causes of the large warm bias in the Angola–Benguela frontal zone in the Norwegian earth system model. *Climate Dynamics*, 50(11-12):4651–4670.

Kozlov, I., Dailidienė, I., Korosov, A., Klemas, V., and Mingėlaitė, T. (2014). MODIS-based sea surface temperature of the Baltic Sea Curonian Lagoon. *Journal of Marine Systems*, 129:157–165.

Locarnini, R., Mishonov, A., Antonov, J., Boyer, T., and Garcia, H. (2006). *World Ocean Atlas 2005, Volume 1: Temperature*. U.S. Government Printing Office, Washington. NOAA Atlas NESDIS 61.

López, M., Zamudio, L., and Padilla, F. (2005). Effects of the 1997–1998 El Niño on the exchange of the northern Gulf of California. *Journal of Geophysical Research: Oceans*, 110(C11).

Lorenc, A., Bell, R., and Macpherson, B. (1991). The Meteorological Office analysis correction data assimilation scheme. *Quarterly Journal of the Royal Meteorological Society*, 117(497):59–89.

Lutjeharms, J. and Meeuwis, J. (1987). The extent and variability of South-East Atlantic upwelling. *South African Journal of Marine Science*, 5(1):51–62.

Lutjeharms, J., Shillington, F., and Duncombe-Rae, C. (1991). Observations of extreme upwelling filaments in the Southeast Atlantic Ocean. *Science*, 253(5021):774.

Lutjeharms, J., Webb, D., De Cuevas, B., and Thompson, S. (1995). Large-scale modelling of the south-east Atlantic upwelling system. *South African Journal of Marine Science*, 16(1):205–225.

Luyt, H. (2016). Evaluating the benefit of assimilating satellite sea surface temperatures in forecasting Benguela upwelling events. Unpublished honours thesis, Stellenbosch University, Stellenbosch.

Lyu, G., Wang, H., Zhu, J., Wang, D., Xie, J., and Liu, G. (2014). Assimilating the along-track sea level anomaly into the regional ocean modeling system using the ensemble optimal interpolation. *Acta Oceanologica Sinica*, 33(7):72.

Machu, E., Goubanova, K., Le Vu, B., Gutknecht, E., and Garçon, V. (2015). Downscaling

biogeochemistry in the Benguela eastern boundary current. *Ocean Modelling*, 90:57–71.

Marsland, S. J., Haak, H., Jungclaus, J. H., Latif, M., and Röske, F. (2003). The Max-Planck-Institute global ocean/sea ice model with orthogonal curvilinear coordinates. *Ocean modelling*, 5(2):91–127.

Martin, M., Hines, A., and Bell, M. (2007). Data assimilation in the FOAM operational short-range ocean forecasting system: a description of the scheme and its impact. *Quarterly Journal of the Royal Meteorological Society*, 133(625):981–995.

Martin, P. J. (2000). Description of the navy coastal ocean model version 1.0. Technical Report NRL/FR/7322–00-9962, Naval Research Lab Stennis Space Center MS.

Martinho, A. S. and Batteen, M. L. (2006). On reducing the slope parameter in terrain-following numerical ocean models. *Ocean Modelling*, 13(2):166–175.

Mason, E., Colas, F., Molemaker, J., Shchepetkin, A. F., Troupin, C., McWilliams, J. C., and Sangrà, P. (2011). Seasonal variability of the Canary Current: a numerical study. *Journal of Geophysical Research: Oceans*, 116(C6).

Mellor, G. L. (1998). Users guide for a three dimensional, primitive equation, numerical ocean model. Technical Report 08544-0710, Program in Atmospheric and Oceanic Sciences, Princeton University Princeton, NJ.

Minnett, P., Evans, R., Kearns, E., and Brown, O. (2002). Sea-surface temperature measured by the Moderate Resolution Imaging Spectroradiometer (MODIS). In *Geoscience and Remote Sensing Symposium, 2002. IGARSS'02. 2002 IEEE International*, volume 2, pages 1177–1179. IEEE.

Minnett, P. J., Brown, O. B., Evans, R. H., Key, E. L., Kearns, E. J., Kilpatrick, K., Kumar, A., Maillet, K. A., and Szczodrak, G. (2004). Sea-surface temperature measurements from the Moderate-Resolution Imaging Spectroradiometer (MODIS) on Aqua and Terra. In *Geoscience and Remote Sensing Symposium, 2004. IGARSS'04. Proceedings. 2004 IEEE International*, volume 7, pages 4576–4579. IEEE.

Mohrholz, V., Bartholomae, C., Van der Plas, A., and Lass, H. (2008). The seasonal variability of the northern Benguela undercurrent and its relation to the oxygen budget on the shelf. *Continental Shelf Research*, 28(3):424–441.

Mohrholz, V., Eggert, A., Junker, T., Nausch, G., Ohde, T., and Schmidt, M. (2014). Cross shelf hydrographic and hydrochemical conditions and their short term variability at the northern Benguela during a normal upwelling season. *Journal of Marine Systems*, 140:92–110.

Mohrholz, V., Schmidt, M., Lutjeharms, J., and John, H.-C. (2004). Space-time behaviour of the Angola-Benguela Frontal Zone during the Benguela Niño of April 1999. *International Journal of Remote Sensing*, 25(7-8):1337–1340.

Moroshkin, K., Bubnov, V., and Bulatov, R. (1970). Water circulation in the eastern South Atlantic Ocean. *Oceanology*, 10(1):27–34.

Mullon, C., Cury, P., and Penven, P. (2002). Evolutionary individual-based model for the recruitment of anchovy (Engraulis capensis) in the southern Benguela. *Canadian Journal of Fisheries and Aquatic Sciences*, 59(5):910–922.

Nelson, G. (1989). Poleward motion in the Benguela area. In *Poleward flows along eastern*

ocean boundaries, pages 110–130. Springer.

Nelson, G. and Hutchings, L. (1983). The Benguela upwelling area. *Progress in Oceanography*, 12(3):333–356.

Nkomo, J. C. (2009). Energy security and liquid fuels in South Africa. *Journal of Energy in Southern Africa*, 20(1):20–24.

Oke, P. R., Allen, J. S., Miller, R. N., Egbert, G. D., and Kosro, P. M. (2002). Assimilation of surface velocity data into a primitive equation coastal ocean model. *Journal of Geophysical Research: Oceans*, 107(C9).

Oke, P. R., Brassington, G. B., Griffin, D. A., and Schiller, A. (2008). The Bluelink ocean data assimilation system (BODAS). *Ocean Modelling*, 21(1):46–70.

Oke, P. R., Sakov, P., and Corney, S. P. (2007). Impacts of localisation in the EnKF and EnOI: experiments with a small model. *Ocean Dynamics*, 57(1):32–45.

Oki, T. (1998). Design of the global river channel network for Total Runoff Integrating Pathways (TRIP). *Earth Interactions*, 2.

Open University (1989). *Ocean Circulation*. Open University and Butterworth-Heinemann, Oxford, 2 edition. Prepared by an Open University course team.

Parada, C., Van Der Lingen, C., Mullon, C., and Penven, P. (2003). Modelling the effect of buoyancy on the transport of anchovy (Engraulis capensis) eggs from spawning to nursery grounds in the southern Benguela: an IBM approach. *Fisheries oceanography*, 12(3):170–184.

Parrish, R., Bakun, A., Husby, D., and Nelson, C. (1983). Comparative climatology of selected environmental processes in relation to eastern boundary current pelagic fish reproduction. In Sharp, G. and Csirke, J., editors, *Proceedings of the Expert Consultation to Examine Changes in Abundance and Species Composition of Neritic Fish Resources. San José. Costa Rica, April 1983*, volume 291, pages 731–777. FAO Fisheries Report.

Pascual, A., Faugère, Y., Larnicol, G., and Le Traon, P.-Y. (2006). Improved description of the ocean mesoscale variability by combining four satellite altimeters. *Geophysical Research Letters*, 33(2).

Penven, P., Claude, R., de Verdière, A. C., and Largier, J. (2000). Simulation of a coastal jet retention process using a barotropic model. *Oceanologica Acta*, 23(5):615–634.

Penven, P., Debreu, L., Marchesiello, P., and McWilliams, J. C. (2006). Evaluation and application of the ROMS 1-way embedding procedure to the central California upwelling system. *Ocean Modelling*, 12(1-2):157–187.

Penven, P., Echevin, V., Pasapera, J., Colas, F., and Tam, J. (2005). Average circulation, seasonal cycle, and mesoscale dynamics of the Peru Current System: A modeling approach. *Journal of Geophysical Research: Oceans*, 110(C10).

Penven, P., Roy, C., Brundrit, G., de Verdière, A. C., Fréon, P., Johnson, A., Lutjeharms, J., and Shillington, F. (2001). A regional hydrodynamic model of the Southern Benguela upwelling. *South African Journal of Science*, 9:472–475.

Pitcher, G. and Calder, D. (2000). Harmful algal blooms of the southern Benguela Current: a review and appraisal of monitoring from 1989 to 1997. *African Journal of Marine Science*, 22.

Preston-Whyte, R. A. and Tyson, P. D. (1988). *Atmosphere and weather of southern Africa*. Oxford University Press.

Qin, H., Chen, G., Wang, W., Wang, D., and Zeng, L. (2014). Validation and application of MODIS-derived SST in the South China Sea. *International journal of remote sensing*, 35(11-12):4315–4328.

Reid, J. L. (1989). On the total geostrophic circulation of the South Atlantic Ocean: Flow patterns, tracers, and transports. *Progress in Oceanography*, 23(3):149–244.

Reinart, A. and Reinhold, M. (2008). Mapping surface temperature in large lakes with MODIS data. *Remote Sensing of Environment*, 112(2):603–611.

Renault, L., McWilliams, J. C., and Penven, P. (2017). Modulation of the Agulhas current retroflection and leakage by oceanic current interaction with the atmosphere in coupled simulations. *Journal of Physical Oceanography*, 47(8):2077–2100.

Roy, C., Weeks, S., Rouault, M., Nelson, G., Barlow, R., and Van der Lingen, C. (2001). Extreme oceanographic events recorded in the Southern Benguela during the 1999–2000 summer season. *South African Journal of Science*, 97(11-12):465–471.

Sakko, A. (1998). The influence of the Benguela upwelling system on Namibia's marine biodiversity. *Biodiversity and Conservation*, 7(4):419–433.

Schiller, R. V. and Kourafalou, V. H. (2010). Modeling river plume dynamics with the HYbrid Coordinate Ocean Model. *Ocean Modelling*, 33(1):101–117.

Schmidt, M. and Eggert, A. (2016). Oxygen cycling in the northern Benguela Upwelling System: Modelling oxygen sources and sinks. *Progress in Oceanography*, 149:145–173.

Shannon, L., Agenbag, J., and Buys, M. (1987). Large- and mesoscale features of the Angola-Benguela front. *South African Journal of Marine Science*, 5(1):11–34.

Shannon, L. and Nelson, G. (1996). The Benguela: large scale features and processes and system variability. In Wefer, G., Berger, W., Siedler, G., and Webb, D., editors, *The South Atlantic*, pages 163–210. Springer, Berlin.

Shannon, L. V. (1985). The Benguela ecosystem. I: Evolution of the Benguela physical features and processes. *Oceanography and Marine Biology*, 23:105–182.

Shannon, L. V. and O'Toole, M. (2003). Sustainability of the Benguela: ex Africa semper aliquid novi. In Sherman, K. and Hempel, G., editors, *Large Marine Ecosystems of the World—Trends in Exploitation, Protection and Research*, pages 227–253. Elsevier, Amsterdam.

Shchepetkin, A. F. and McWilliams, J. C. (2005). The regional oceanic modeling system (ROMS): a split-explicit, free-surface, topography-following-coordinate oceanic model. *Ocean modelling*, 9(4):347–404.

Shillington, F., Hutchings, L., Probyn, T., Waldron, H., and Peterson, W. (1992). Filaments and the Benguela frontal zone: offshore advection or recirculating loops? *South African Journal of Marine Science*, 12(1):207–218.

Shinoda, T. and Lin, J. (2009). Interannual variability of the upper ocean in the southeast Pacific stratus cloud region. *Journal of Climate*, 22(19):5072–5088.

Shulman, I., Rowley, C., Anderson, S., DeRada, S., Kindle, J., Martin, P., Doyle, J., Cummings, J., Ramp, S., Chavez, F., et al. (2009). Impact of glider data assimilation on

the Monterey Bay model. *Deep Sea Research Part II: Topical Studies in Oceanography*, 56(3-5):188–198.

Shulman, I., Wu, C.-R., Lewis, J., Paduan, J., Rosenfeld, L., Kindle, J., Ramp, S., and Collins, C. (2002). High resolution modeling and data assimilation in the Monterey Bay area. *Continental Shelf Research*, 22(8):1129–1151.

Skamarock, W., Klemp, J., Dudhia, J., Gill, D., Barker, D., Duda, M., Huang, X., Wang, W., and Powers, J. (2008). A description of the Advanced Research WRF Version 3. Technical Report NCAR/TN-475, National Center for Atmospheric Research.

Skogen, M. (1999). A biophysical model applied to the Benguela upwelling system. *African Journal of Marine Science*, 21.

Skogen, M. and Søiland, H. (1998). A user's guide to NORWECOM v. 2.0. The Norwegian ecological model system. *Fisken og Havet*, 18(42):1–2.

Song, Y. and Haidvogel, D. (1994). A semi-implicit ocean circulation model using a generalized topography-following coordinate system. *Journal of Computational Physics*, 115(1):228–244.

Srinivasan, A., Chassignet, E., Bertino, L., Brankart, J., Brasseur, P., Chin, T., Counillon, F., Cummings, J., Mariano, A., Smedstad, O., et al. (2011). A comparison of sequential assimilation schemes for ocean prediction with the HYbrid Coordinate Ocean Model (HYCOM): Twin experiments with static forecast error covariances. *Ocean Modelling*, 37(3):85–111.

Stander, G. (1964). The Benguela Current off South West Africa. *Investl. Rep. mar. Res. Lab. SW Afr.*, 12:43.

Stevens, I. and Johnson, J. (2003). A numerical modelling study of upwelling filaments off the NW African coast. *Oceanologica acta*, 26(5-6):549–564.

Strub, P., Shillington, F., James, C., and Weeks, S. (1998). Satellite comparison of the seasonal circulation in the Benguela and California current systems. *South African Journal of Marine Science*, 19(1):99–112.

Talley, L. D., Pickard, G. L., Emery, W. J., and Swift, J. H. (2011). *Descriptive Physical Oceanography: An Introduction*. Academic press, 6 edition.

Tim, N., Zorita, E., and Hünicke, B. (2015). Decadal variability and trends of the Benguela upwelling system as simulated in a high-resolution ocean simulation. *Ocean Science*, 11(3):483–502.

Traon, P. and Dibarboure, G. (2004). An illustration of the contribution of the TOPEX/Poseidon—Jason-1 tandem mission to mesoscale variability studies. *Marine Geodesy*, 27(1-2):3–13.

Troupin, C., Mason, E., Beckers, J.-M., and Sangrà, P. (2012). Generation of the Cape Ghir upwelling filament: A numerical study. *Ocean Modelling*, 41:1–15.

van Foreest, D. and Brundrit, G. (1982). A two-mode numerical model with applications to coastal upwelling. *Progress In Oceanography*, 11:329–392.

Veitch, J., Penven, P., and Shillington, F. (2009). The Benguela: A laboratory for comparative modeling studies. *Progress in Oceanography*, 83(1):296–302.

Veitch, J., Penven, P., and Shillington, F. (2010). Modeling equilibrium dynamics of the

Benguela Current System. *Journal of Physical Oceanography*, 40(9):1942–1964.

Veitch, J. A. and Penven, P. (2017). The role of the Agulhas in the Benguela Current system: A numerical modeling approach. *Journal of Geophysical Research: Oceans*.

Wallcraft, A., Metzger, E., and Carroll, S. (2009). Software design description for the hybrid coordinate ocean model (HYCOM), version 2.2. Technical report, Naval Research Lab Stennis Space Center MS Oceanography Div.

Wan, L., Bertino, L., and Zhu, J. (2010). Assimilating altimetry data into a HYCOM model of the Pacific: Ensemble Optimal Interpolation versus Ensemble Kalman Filter. *Journal of Atmospheric and Oceanic Technology*, 27(4):753–765.

Weeks, S., Barlow, R., Roy, C., and Shillington, F. (2006). Remotely sensed variability of temperature and chlorophyll in the southern Benguela: upwelling frequency and phytoplankton response. *African Journal of Marine Science*, 28(3-4):493–509.

Wunsch, C. and Stammer, D. (1998). Satellite altimetry, the marine geoid, and the oceanic general circulation. *Annual Review of Earth and Planetary Sciences*, 26(1):219–253.

Xie, J., Counillon, F., Zhu, J., and Bertino, L. (2011). An eddy resolving tidal-driven model of the South China Sea assimilating along-track SLA data using the EnOI. *Ocean Science*, 7(5):609–627.

Xie, J. and Zhu, J. (2010). Ensemble optimal interpolation schemes for assimilating Argo profiles into a hybrid coordinate ocean model. *Ocean Modelling*, 33(3):283–298.

Zamudio, L., Hogan, P., and Metzger, E. J. (2008). Summer generation of the Southern Gulf of California eddy train. *Journal of Geophysical Research: Oceans*, 113(C6).

Zamudio, L., Metzger, E. J., and Hogan, P. (2011). Modeling the seasonal and interannual variability of the northern Gulf of California salinity. *Journal of Geophysical Research: Oceans*, 116(C2).

Zamudio, L., Metzger, E. J., and Hogan, P. J. (2010). Gulf of California response to hurricane Juliette. *Ocean Modelling*, 33(1-2):20–32.

Appendix A

Seasonal increments

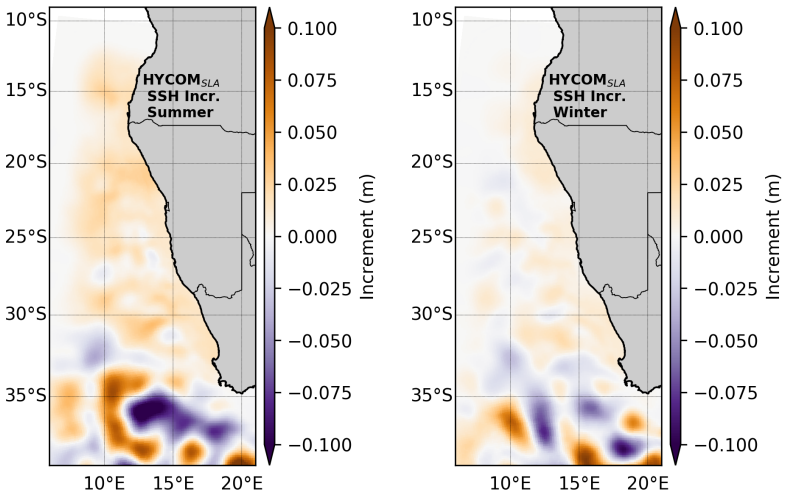

(a) HYCOM$_{\mathrm{SLA}}$.

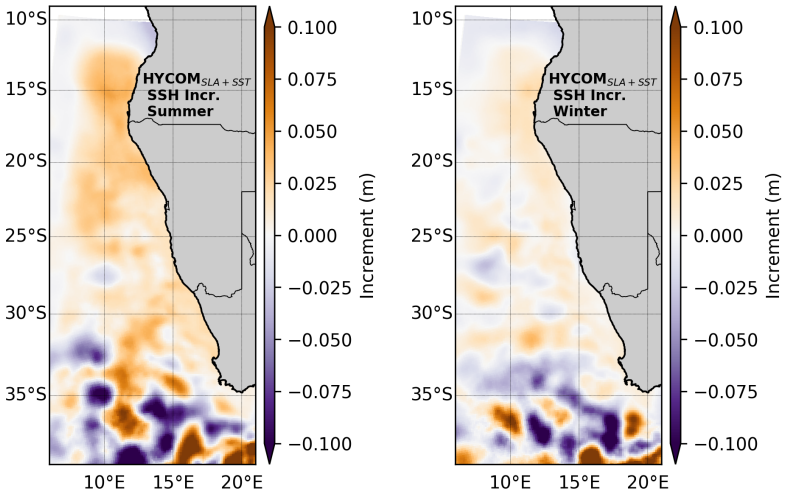

(b) HYCOM$_{\mathrm{SLA+SST}}$.

Figure A.1: SSH seasonal increments in **(a)** HYCOM$_{\mathrm{SLA}}$ and **(b)** HYCOM$_{\mathrm{SLA+SST}}$, 2008–2009.

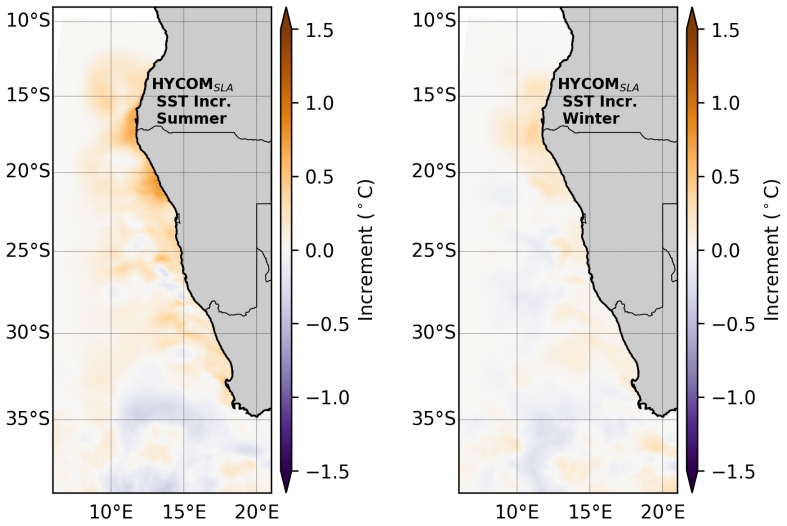

(a) HYCOM$_{\mathrm{SLA}}$.

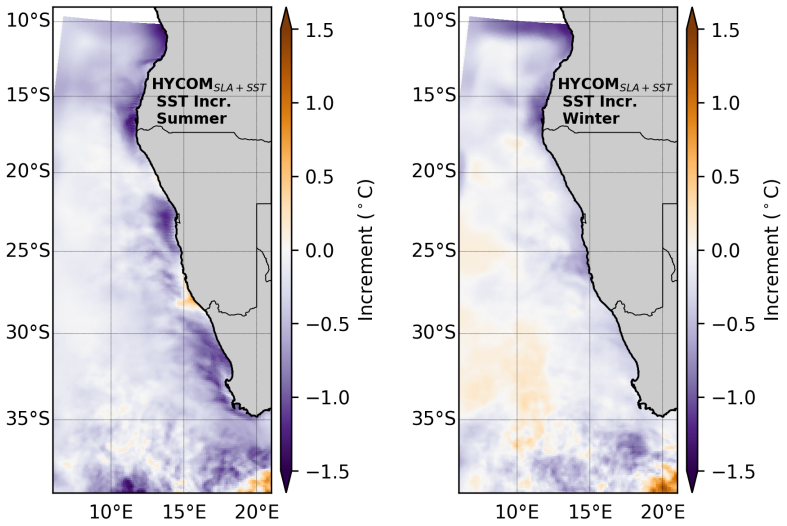

(b) HYCOM$_{\mathrm{SLA+SST}}$.

Figure A.2: SST seasonal increments in **(a)** HYCOM$_{\mathrm{SLA}}$ and **(b)** HYCOM$_{\mathrm{SLA+SST}}$, 2008–2009.

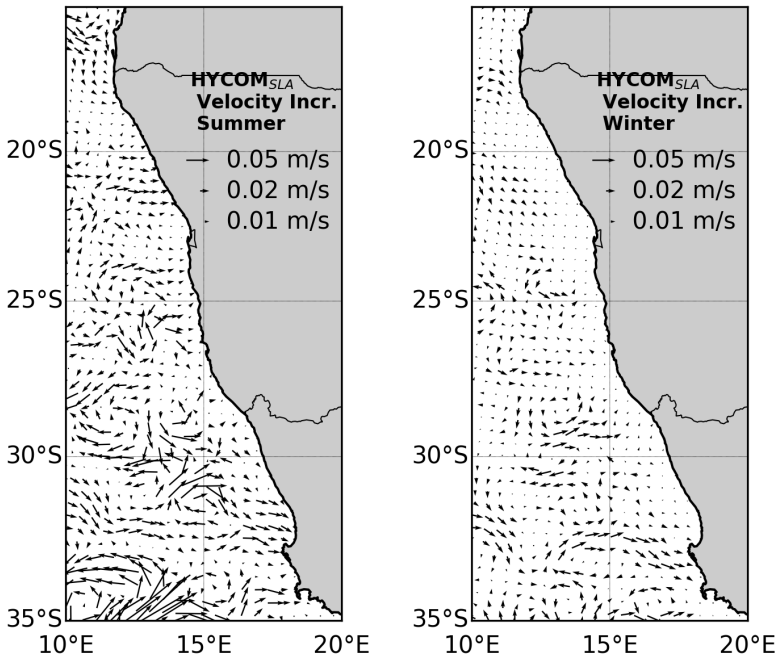

(a) $\mathrm{HYCOM_{SLA}}$.

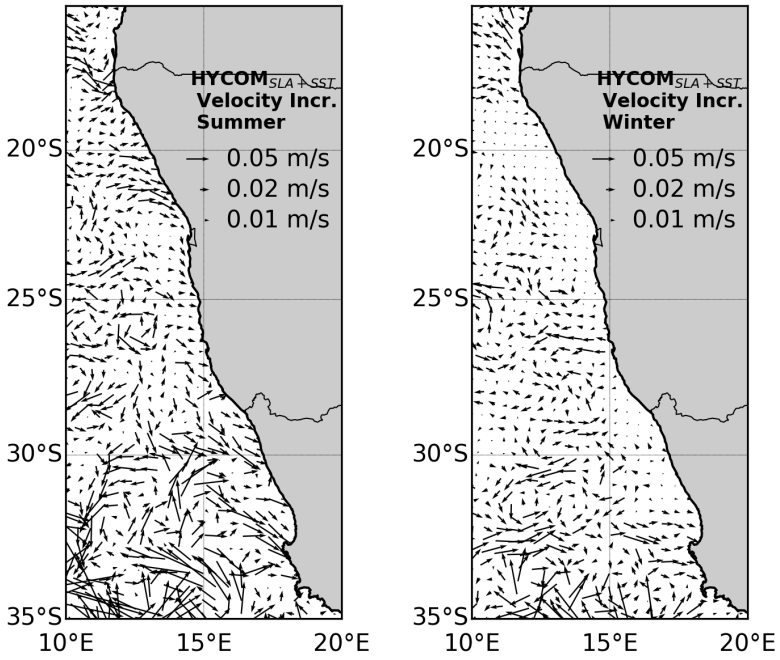

(b) $\mathrm{HYCOM_{SLA+SST}}$.

Figure A.3: Surface velocity seasonal increments in **(a)** $\mathrm{HYCOM_{SLA}}$ and **(b)** $\mathrm{HYCOM_{SLA+SST}}$, 2008–2009.